Department of Micro- and Nanosciences

Low energy electron beam irradiation of gallium nitride

Henri Tapio Nykänen

A!

DOCTORAL DISSERTATIONS

Aalto University publication series
DOCTORAL DISSERTATIONS 190/2013

Low energy electron beam irradiation of gallium nitride

Henri Tapio Nykänen

A doctoral dissertation completed for the degree of Doctor of Science (Technology) (Doctor of Philosophy) to be defended, with the permission of the Aalto University School of Electrical Engineering, at a public examination held in large seminar room at Micronova-building (Tietotie 3, Espoo, Finland) on 20th December 2013 at 12.

Aalto University
School of Electrical Engineering
Department of Micro- and Nanosciences
Optoelectronics

Supervising professor
Markku Sopanen

Preliminary examiners
Professor Kai Nordlund (Helsinki University, Finland)
Professor Robert Martin (University of Strathclyde, United Kingdom)

Opponent
Doctor Michelle Moram (Imperial College London, U.K.)

Aalto University publication series
DOCTORAL DISSERTATIONS 190/2013

ISBN 978-952-60-5444-5
ISBN 978-952-60-5445-2 (pdf)
ISSN-L 1799-4934
ISSN 1799-4934 (printed)
ISSN 1799-4942 (pdf)
http://urn.fi/URN:ISBN:978-952-60-5445-2

Unigrafia Oy
Helsinki 2013

Finland

441 697
Printed matter

Aalto University

Abstract

Aalto University, P.O. Box 11000, FI-00076 Aalto www.aalto.fi

Author
Henri Tapio Nykänen

Name of the doctoral dissertation
Low energy electron beam irradiation of gallium nitride

Publisher School of Electrical Engineering

Unit Department of Micro- and Nanosciences

Series Aalto University publication series DOCTORAL DISSERTATIONS 190/2013

Field of research Optical materials

Manuscript submitted 21 August 2013 **Date of the defence** 20 December 2013

Permission to publish granted (date) 25 October 2013 **Language** English

☐ **Monograph** ☒ **Article dissertation (summary + original articles)**

Abstract

In this work, the behavior of gallium nitride and indium gallium nitride under low energy electron beam irradiation (LEEBI) has been investigated. Furthermore, a periodic silver grating has been investigated and fabricated with the aim of obtaining plasmonic coupling based luminescence enhancement from a light emitting structure. The effect of the silver grating and LEEBI were both studied using photoluminescence (PL) measurements and the silver grating properties were also investigated using reflectometry.

It has been observed in this work that LEEBI causes significant degradation of band-edge (BE) luminescence in metal-organic vapor phase epitaxy (MOVPE) grown InGaN quantum well (QW) structures and GaN films. The degradation increases with increasing LEEBI dose (charge per surface area). Moreover, the PL intensity decreases faster with smaller kinetic energy of electrons. This in agreement with the electron beam energy dissipation profile in GaN.

The mechanism of the BE luminescence degradation has been studied with positron annihilation spectroscopy (PAS). The measurements reveal that LEEBI is able to activate in-grown gallium vacancies (V_{Ga}) in GaN, which are otherwise passive, i.e., neutral through the band gap and invisible to PAS. The mechanism for the passivation of the V_{Ga} is the formation of vacancy - hydrogen complexes, especially V_{Ga} - 3H. Hence, LEEBI treatment can probably remove hydrogen from these complexes making them active. Moreover, LEEBI induced optical degradation was measured to be virtually identical for samples grown in both hydrogen and nitrogen environments. Also, a partial recovery of the BE emission was obtained with thermal annealing. This suggests internal migration of H, partially refilling the vacancy sites.

A silver nano-grating structure covered with (poly)vinyl alcohol (PVA), deposited on top of an InGaN QW structure, was developed. The buried metal grating can diffract light from the optical modes propagating in GaN and PVA. This simple technique has already yielded emitted light intensity almost 3-fold the original.

Keywords gallium nitride, electron beam irradiation, optical degradation

ISBN (printed) 978-952-60-5444-5 **ISBN (pdf)** 978-952-60-5445-2

ISSN-L 1799-4934 **ISSN (printed)** 1799-4934 **ISSN (pdf)** 1799-4942

Location of publisher Helsinki **Location of printing** Helsinki **Year** 2013

Pages 71 **urn** http://urn.fi/URN:ISBN:978-952-60-5445-2

Tekijä
Henri Tapio Nykänen

Väitöskirjan nimi
Galliumnitridin säteilytys matalaenergisellä elektronisuihkulla

Julkaisija Sähkötekniikan korkeakoulu

Yksikkö Mikro- ja nanotekniikan laitos

Sarja Aalto University publication series DOCTORAL DISSERTATIONS 190/2013

Tutkimusala Optiset materiaalit

Käsikirjoituksen pvm 21.08.2013 **Väitöspäivä** 20.12.2013

Julkaisuluvan myöntämispäivä 25.10.2013 **Kieli** Englanti

☐ **Monografia** ☒ **Yhdistelmäväitöskirja (yhteenveto-osa + erillisartikkelit)**

Tiivistelmä

Tässä työssä on tutkittu galliumnitridin ja indiumgalliumnitridin käyttäytymistä kun niitä säteilytetään matalaenergisella elektronisuihkulla (engl., low energy electron beam irradiation, LEEBI). Tämän lisäksi tutkittiin ja valmistettiin periodisia hopearaidoituksia, jonka tavoitteena oli aikaansaada plasmonikytkentään perustuva valon emission lisäys. Sekä hopearaitojen, että LEEBI:n vaikutusta tutkittiin fotoluminesenssiin (engl., photoluminescence, PL) perustuvin mittauksin. Lisäksi hopearaitojen ominaisuuksia mitattiin käyttäen reflektometriaa.

On osoitettu, että LEEBI aiheuttaa selvän vaimenemisen valon emission intensiteetissä metallo-orgaanisella kaasufaasiepitaksialla valmistetuissa InGaN kvanttikaivoissa (engl., quantum well, QW) sekä GaN-kalvoissa. Vaimeneminen on voimakkaampaa LEEBI-säteilyannoksen kasvaessa. Vaimeneminen on myös voimakkaampaa pienemmillä elektronien liike-energioilla. Tämä täsmää hyvin elektronisäteen energian tunkeutumisprofiilin kanssa.

Vaimenemisen aiheuttavaa mekanismia on tutkittu positroniannihilaatiospektroskopialla (PAS). Mittaukset paljastavat, että LEEBI aktivoi valmistuksen aikana muodostuneita galliumvakansseja (V_{Ga}), jotka ovat muuten passiivisia. Toisin sanoen ne eivät vaikuta PL-signaaliin eivätkä näy PAS:ssa. Vakanssien passivaatiomekanismismi liittynee kompleksien muodostumiseen vedyn kanssa. Erityisesti V_{Ga} -3H kompleksi ei näy PAS-mittauksissa ja on neutraali. Koska vaimeneminen on identtistä näytteiden välillä, jotka on kasvatettu vedyssä ja typessä, voidaan todeta että vedyn lähde ei ole kantajakaasu. Näytteiden lämmittäminen palauttaa osan luminesenssin intensiteetistä. Todennäköisesti näytteen sisäinen vetydiffuusio uudelleenpassivoi vakansseja.

Olemme kehittäneet pintarakenteen (poly)vinyyliakoholilla (PVA) peitetyistä hopeananoraidoista InGaN QW-rakenteen päälle. Hopearaidat voivat difraktoida valokanavamoodeja GaN- ja PVA-kerroksista, lisäten näin merkittävästi valon ulospääsyä rakenteesta. Tällä yksinkertaisella tekniikalla on saavutettu lähes 3-kertainen valon intensiteetti verrattuna käsittelemättömään näytteeseen.

Avainsanat galliumnitridi, elektronisäteily, optinen laatu

ISBN (painettu) 978-952-60-5444-5 **ISBN (pdf)** 978-952-60-5445-2

ISSN-L 1799-4934 **ISSN (painettu)** 1799-4934 **ISSN (pdf)** 1799-4942

Julkaisupaikka Helsinki **Painopaikka** Helsinki **Vuosi** 2013

Sivumäärä 71 **urn** http://urn.fi/URN:ISBN:978-952-60-5445-2

Preface

This work was carried out at the Department of Micro- and Nanosciences, School of Electrical Engineering, Aalto University, between 2009 and 2013.

I wish to express my sincere gratitude to professor Markku Sopanen for supervising my thesis and for giving me an opportunity to work with many interesting subjects. The research in field of optoelectronics has been truly interesting and the experience gained during this work is sure to greatly benefit me in the future.

I would like to thank Prof. Harri Lipsanen, Prof. Filip Tuomisto, Dr. Sami Suihkonen, Dr. Juha Riikonen, M.Sc. Olli Svensk, M. Sc. Lauri Riuttanen and M. Sc. Päivi Mattila for their contribution, help and friendship during my thesis work. It has been a pleasure to work with such good people. I have learned a lot from all of you.

I would also like to thank my collaboration partners Professor Joel Bellessa, Dr. Estelle Homeyer and Dr. Yohjiro Kawai for their contribution to our research together. Keep up the good work!

Finally, I want to extend my gratitude to my mother, who has always supported me all my life, and to my wife Jana for warm loving feelings and keeping me on my path.

Helsinki, November 5, 2013,

Henri Tapio Nykänen

Contents

List of Publications

This thesis consists of an overview and of the following publications which are referred to in the text by their Roman numerals.

I H. Nykänen, P. Mattila, S. Suihkonen, J. Riikonen, E. Quillet, E. Homeyer, J. Bellessa, and M. Sopanen. Low energy electron beam induced damage on InGaN/GaN quantum well structure. *Journal of Applied Physics*, 109, 083105, 2011.

II H. Nykänen, P. Mattila, S. Suihkonen, J. Riikonen, and M. Sopanen. Low energy electron beam induced damage on gallium nitride based materials. *Physica Status Solidi C*, 9, 7, 1563-1565, 2012.

III H. Nykänen, S. Suihkonen, L. Kilanski, M. Sopanen, and F. Tuomisto. Low energy electron beam induced vacancy activation in GaN. *Applied Physics Letters*, 100, 122105, 2012.

IV H. Nykänen, S. Suihkonen, M. Sopanen and F. Tuomisto. Thermally assisted recovery of low energy electron beam irradiation in-duced optical degradation of GaN. *Physica Status Solidi C*, 10,461-463, 2013.

V S. Suihkonen, H. Nykänen, T. Tanikawa, M. Yamaguchi, Y. Honda, and H. Amano. Effects of low energy e-beam irradiation on cathodoluminescence from GaN. *Physica Status Solidi A*, 210, 2, 383-385, 2013.

VI E. Homeyer, P. Mattila, J. Oksanen, T. Sadi, H. Nykänen, S. Suihkonen,

C. Symonds, J. Tulkki, F. Tuomisto, M. Sopanen, and J. Bellessa. Enhanced light extraction from InGaN/GaN quantum well with silver gratings. *Applied Physics Letters*, 102, 8, 081110, 2013.

VII H. Nykänen, S. Suihkonen, O. Svensk, M. Sopanen and F. Tuomisto. Band-edge Luminescence Degradation by Low Energy Electron Beam Irradiation in MOVPE GaN Grown in H_2 and N_2 Ambients. *Japanese Journal of Applied Physics*, submitted, 2013.

Author's Contribution

Publication I: "Low energy electron beam induced damage on InGaN/GaN quantum well structure"

The author wrote the manuscript of this publication. The author designed and carried out the experiments, including most of sample preparation and electron beam exposure. The author carried out the photoluminescence measurements, and analyzed the results.

Publication II: "Low energy electron beam induced damage on gallium nitride based materials"

The author wrote the manuscript of this publication. The author designed and carried out the experiments including most of sample preparation and electron beam exposure. The author performed the measurements, and analyzed the results.

Publication III: "Low energy electron beam induced vacancy activation in GaN"

The author wrote the manuscript of this publication. The author designed and carried out the experiments, including most of sample preparation and electron beam exposure. The author performed the photoluminescence measurements and analyzed the results with the co-authors.

Publication IV: "Thermally assisted recovery of low energy electron beam irradiation in-duced optical degradation of GaN"

The author wrote the manuscript of this publication. The author designed and carried out the experiments, including most of sample preparation, electron beam exposure and annealing. The author carried out the photoluminesncence measurements, and analyzed the results.

Publication V: "Effects of low energy e-beam irradiation on cathodoluminescence from GaN"

The author wrote a part of the manuscript and assisted in sample preparation and measurements with the co-authors.The author also assisted with the result analysis.

Publication VI: "Enhanced light extraction from InGaN/GaN quantum well with silver gratings"

The author fabricated the samples with the co-authors and assisted in the measurements, analysis and manuscript preparation.

Publication VII: "Band-edge Luminescence Degradation by Low Energy Electron Beam Irradiation in MOVPE GaN Grown in H_2 and N_2 Ambients"

The author wrote the manuscript of this publication. The author designed and carried out the experiments, including most of sample preparation and electron beam exposure. The author performed the photoluminescence measurements and analyzed the results with the co-authors.

List of Abbreviations

AlGaN	aluminum gallium nitride
BE	band-edge
BL	blue luminescence
CL	cathodoluminescence
DLTS	deep-level transient spectroscopy
e-beam	electron beam
EBIC	electron beam induced current
EBL	electron beam lithography
EDX	energy-dispersive X-ray spectroscopy
FWHM	full width at half maximum
GaN	gallium nitride
HVPE	hydride vapor phase epitaxy
InGaN	indium gallium nitride
LED	light emitting diode
LEEBI	low energy electron beam irradiation
LD	laser diode
MBE	molecular beam epitaxy
MOVPE	metal-organic vapor phase epitaxy
MQW	multiple quantum well
PAS	positron annihilation spectroscopy

PL	photoluminescence
PMMA	(poly)methyl methacrylate
PVA	polyvinyl alcohol
QW	quantum well
RT	room temperature
SEM	scanning electron microscopy
SQW	single quantum well
TE	transverse electric
TEM	transmission electron microscopy
TM	transverse magnetic
UV	ultra violet
V_{Ga}	gallium vacancy
V_N	nitrogen vacancy
YL	yellow luminescence

1. Introduction

The first light emitting diode (LED) was created by Russian Oleg Losev in 1927 [1]. However, this invention did not become well known for many years. In 1955 R. Braunstein observed infrared radiation from certain semiconductor materials, *e.g.*, gallium arsenide and indium phosphide [2]. The first useful LED emitting red light was developed in 1962 by N. Holonyak, who is considered to be the father of the modern LED [3]. The first highly efficient blue LED was made by S. Nakamura from indium gallium nitride in 1994.

Nowadays, LEDs and laser diodes (LD) are a group of optoelectronic components utilized in numerous applications. They are used in energy efficient lightning, optical communications, industrial processes and measurement devices, just to mention a few examples [4–8]. Depending on the application, different emission wavelengths (*i.e.*, light colors) are needed. The realizations require different kinds of semiconductor materials with different electrical and optical properties.

Gallium nitride (GaN) is probably the most commonly used material in the field of blue and ultraviolet (UV) light emitting devices [9–11]. The possibility to tune the emission wavelength of GaN-based alloys, InGaN for example, also allows fabrication of green light emitting devices and solar cells [12–15]. GaN has numerous advantageous properties. It is a chemically and mechanically hard material which allows it to endure rough environments [16, 17]. It can withstand high current densities and temperatures, which allows high speed and high power operations [18–20]. It is considered to be radiation resistant, making it suitable for, *e.g.*, space applications [12, 21].

In semiconductor fabrication and characterization, low energy electron beam irradiation (LEEBI) based methods are very common. These include, *e.g.*, electron beam induced current (EBIC), scanning electron microscopy (SEM),

electron beam lithography (EBL) and cathodoluminescence (CL). Other electron beam (e-beam) based methods are, *e.g.*, transmission electron microscopy (TEM) and high-energy EBL. The small wavelength of electrons allows much better spatial resolution than conventional UV-light based lithography, hence allowing to image and fabricate smaller structures.

Originally in this work, EBL was used to fabricate nano-scale silver stripes on top of GaN/InGaN/GaN near-surface quantum wells (QWs). The goal was to fabricate a patterning that would significantly enhance light extraction from GaN-based structures. However, when luminescence was measured from a spot that had been EBL-patterned, but not metalized, the luminescence had actually decreased compared to the surrounding areas. This effect was not expected since EBL was thought to be non-destructive and GaN should be relatively resistant to radiation in general.

In this work, effects of LEEBI on InGaN/GaN QWs and epitaxial GaN-films are studied. It has been shown that LEEBI can cause severe damage to the optical properties in both systems. A mechanism proposed to be responsible for this optical degradation is activation of point defects, namely in-grown gallium vacancies (V_{Ga}), in the GaN lattice. Furthermore, the activation mechanism is suggested to be related to removal of hydrogen from the vacancy sites. The results on the fabricated silver nano-gratings on top of InGaN QWs are also presented.

A short introduction to gallium nitride based materials is given in chapter 2, focusing mainly on optical transition mechanisms. Interaction of electron beam radiation with gallium nitride material is discussed in the third chapter in more detail. The fourth chapter describes the fabrication and characterization methods and equipment used in this work. The fifth chapter is dedicated to the main results and discussion of the LEEBI induced degradation. Chapter six describes the extraction enhancement gained using the silver nano-gratings on top of the InGaN QW. Finally a short summary is given in chapter seven. The publications are attached in the end of the thesis.

2. Gallium Nitride Semiconductor

Gallium nitride (GaN) is a III-V group binary compound material that has several advantages in certain fields of semiconductor applications. The main properties of GaN are briefly described in this chapter.

2.1 Fundamental Properties

The functionality of a crystalline semiconductor arises from the organized lattice structure; the atoms form a continuous periodic system with a certain composition. Atoms are connected to each other forming a unit cell which then repeats throughout the whole body. The atoms in the unit cell can be positioned in different ways resulting in different lattice types and hence different semiconductor properties in each case [22].

From the possible lattice types of gallium nitride, wurtzite is the most commonly utilized one in optoelectronics. In wurtzite GaN, the atoms are tetrahedrally bonded to their neighbors, as illustrated in figure 2.1a. Wurtzite GaN is a direct band gap material (see figure 2.1b). Using a direct band gap material allows fabrication of more efficient light emitting devices, compared to materials with an indirect band gap.

Moreover, GaN is a mechanically and chemically hard material. It also has a high heat capacity and thermal conductivity [23–25] making it suitable for high power and high frequency applications. GaN can withstand ionizing radiation better that many other semiconductor materials, making it a good option for, *e.g.*, space and solar cell use [12, 26, 27].

Optical and electrical properties of GaN can be changed via doping to turn the material into p- or n-type semiconductor. This is a necessary feature in semiconductor device fabrication. Magnesium is virtually the only useful

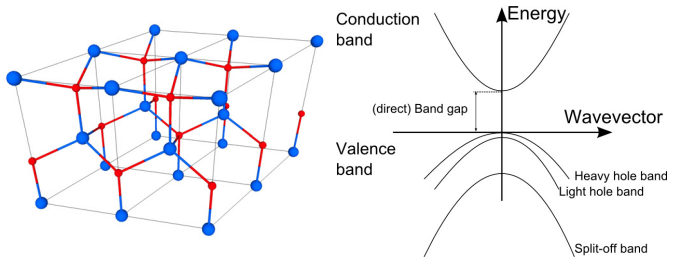

Figure 2.1. a) Illustration of wurtzite GaN lattice. Ga atoms are represented as blue balls and N atoms as red balls. The top plane is parallel to the 0001 (c-plane) direction. b) Illustration of a semiconductor energy band structure with a direct band gap. Bands for holes with different effective masses (heavy, light and split-off) are also shown.

dopant to form p-type GaN [28, 29]. Silicon is most commonly used as the n-type dopant [30, 31]. Chemical compounds accommodating the dopant atoms can be introduced to the GaN growth environment to form p- and n-doping. Doping of GaN is discussed more in section 2.7.

GaN has also other interesting properties. A negative electron affinity can be obtained and used in high brightness photocathodes [32, 33]. Transferred-electron effect (Gunn effect) can be utilized in microwave devices [34]. Pyroelectricity and piezoelectricity are useful in, *e.g.*, sensor applications [35–37, 34].

Free standing GaN is troublesome to obtain directly. Aside from, *e.g.*, ammonothermal method, GaN is grown epitaxially on a foreign substrate material. The substrate is placed in a growth environment with necessary source materials, temperature and pressure. When the conditions are favorable, GaN begins to crystallize on the template, inheriting the crystalline structure of the template material. However, the substrate and GaN typically have different lattice parameters resulting in tensions in the grown film, which again results in defects when the tensions forcefully relax. Furthermore, a large amount of stress rises from the thermal expansion differences (between substrate and grown layer) during the sample cool down. The most commonly used methods for epitaxial growth of GaN include metal-organic vapor phase epitaxy (MOVPE), molecular beam epitaxy (MBE) and hydride vapor phase epitaxy (HVPE). Typical substrate materials are sapphire (Al_2O_3) and silicon carbide (SiC).

2.2 Semiconductor Properties

It follows from the Schrödinger equation [38–40], that perfectly crystalline solid material, due to its periodical lattice structure, will have an electron band structure: the discrete energy levels of electrons bound to atoms broaden to form (virtually) continuous bands of allowed energies. The bands are separated by band gaps [41].

From the band structure, two possible cases arise. Firstly, an allowed energy band is completely filled with electrons, but the next band is completely empty (at 0 K). Secondly, the highest band containing electrons is partially filled. Electrons belonging to a completely filled band cannot carry any current, since electrons (being fermions) can only move to an unoccupied state. Hence, in a totally filled band, there is no net flow of charge. Therefore, materials belonging to the first group, are insulators or semiconductors and materials in the second group are conductors (metals). The band that is filled with electrons (in 0 K) is called the valence band and the empty band above it is called the conduction band. At 0 K, the conductivity of a semiconductor or insulator is zero [41].

The conduction band being empty and the valance band being full only applies in absolute zero for perfect semiconductor. At higher temperatures, some electrons are excited to the conduction band. As a result, there are some unoccupied states in the valence band and some occupied states in the conduction band. An unoccupied state in the valence band is called a hole. In an applied electric field holes move to the opposite direction compared to electrons. Thus, a hole behaves as a positive charge. When an electron is missing from the valence band and is occupying a state in the conduction band, current can flow [41].

At finite temperatures, there always exists some energy in the system (*e.g.*, thermal energy k_BT) which can excite electrons from the valence band to the conduction band, hence leaving a hole in the valence band. The creation of electron-hole pairs is the key for semiconductor usage in optical devices. In photon irradiation, photons with sufficient energy are absorbed and their energy is transferred to valence band electrons, which are then excited to the conduction band. The necessary energy minimum is the width of the band gap. In indirect band gap materials, an additional source of momentum (*e.g.*, a phonon) is necessary due to the rule of momentum conservation [22].

The process reverse to the electron-hole pair excitation is called recombination. An electron in the conduction band minimum recombining with a hole in the valence band maximum is typically denoted as band-edge (BE) recombination. The excess energy is released in radiative or non-radiative manner. In non-radiative recombination the excess energy is usually dissipated as phonons, *i.e.*, as heat. In radiative recombination, the excess energy is transferred to a photon with an energy most often equal or close to the band gap energy. For example, in photoluminescence (see section 4.2) the excitation - recombination process is employed to gain information about the band structure [22]. The absorption and recombination process is illustrated in figure 2.2.

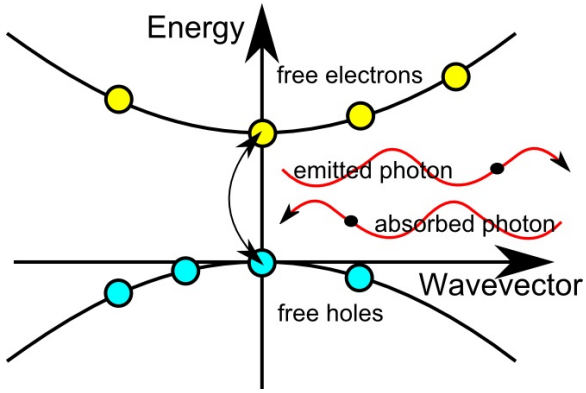

Figure 2.2. Illustration of electron-hole generation by photon absorption and recombination induced photon emission.

In optoelectronic devices, such as LEDs or LDs, free electrons and holes can be injected from a current source by an applied bias voltage. The injected carriers can then recombine emitting photons (or phonons). The emitted radiation is characteristic to the used materials and structures. A part of the electrons and holes can pass through the system without recombining, which lowers the efficiency of the optical emission [22].

In efficient optoelectronic devices, carrier confinement is necessary. The free charge carriers should be bound to the actively emitting region of the structure, so that the major part of the recombination happens within the desired energy regime and without the carriers flowing past the active region. For this reason, heterojunction structures are normally used. These can be fabricated, *e.g.*, by using alloys such as $In_xGa_{(1-x)}N$ and $Al_xGa_{(1-x)}N$. The band gap width is tunable by varying the alloy percentage x. This allows a potential well area to be made for carrier confinement. The tunable band gap width also makes fabrication of different emission wavelength devices possible. A commonly used structure for blue- and UV-emitting device is a multiple quantum well

(MQW) stack of InGaN and GaN sandwiched between p- and n-GaN junction. The electrically injected free carriers diffuse to the junction area where they are confined to the QWs (as illustrated in figure 2.3.). The allowed electron states in the QWs are well defined, resulting in a slightly sharper emission spectrum with higher efficiency of the device [39].

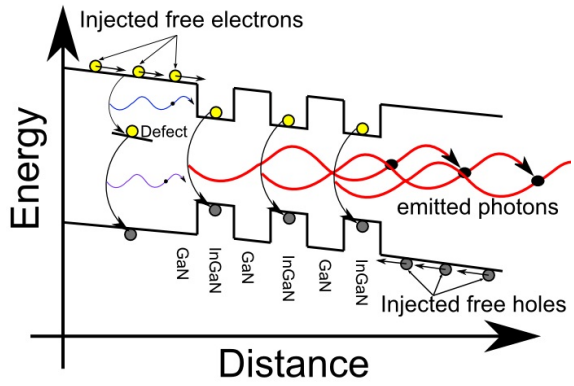

Figure 2.3. Illustration of photon emission in InGaN/GaN MQW stack structure. Also unwanted emission from a defect in the GaN band gap is illustrated.

Another benefit of the heterostructure arises from negligible reabsorption of emitted light. When the band gap of the surrounding material is equal to the band gap of the active region, the emitted photons have a significant probability to be reabsorbed before leaving the material. This limits the efficiency of the device. In heterostructures, the potential well area emits photons with energy smaller than the band gap of the surrounding areas. Hence, these photons leaving the active region are not easily reabsorbed.

2.3 Defects in Crystals

In the perfect case, the semiconductor lattice is infinitely continuous and pure resulting in an ideal energy band structure. However, in practice the lattice will always include unintentional defects and, obviously, terminating surfaces. Defects are caused either by a deformed lattice (*e.g.*, dislocations, figure 2.4b,f,g) or by contamination (impurities, figure 2.4e,h). The defects break the continuous lattice and can form unwanted energy states inside the forbidden band gap [42–44]. Furthermore, some unintentional defects can act as donors or acceptors introducing free carriers [42, 45–48]. Thus, defects can cause unintentional emission wavelengths, non-radiative recombination, unexpected electrical properties and efficiency variations [49, 50]. This is illustrated in

figure 2.5.

Most III-V group semiconductor devices are epitaxially grown. In an epitaxial process, the grown material inherits the crystalline structure of the underlying template. However, for GaN there are no perfect (foreign) template materials, *i.e.*, the template and the grown film have a (often relatively large) mismatch between their lattice constants. This mismatch leads to tensions in the lattice, that are relaxed by deformation. The deformation can extend along the material resulting in a ribbon-like dislocation. For GaN the dislocations are an important defect type causing non-radiative recombination in optoelectronic devices [51].

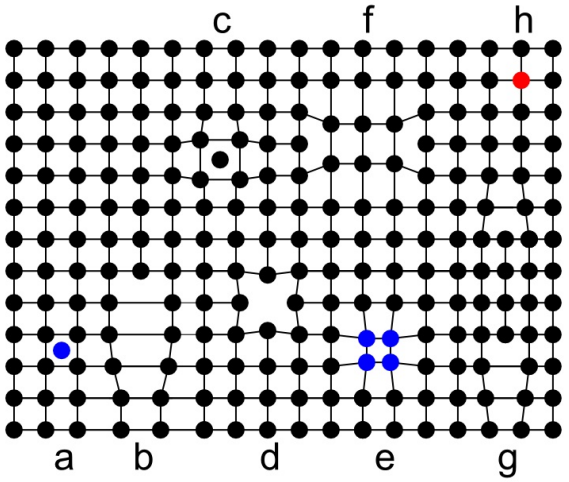

Figure 2.4. Illustration of possible lattice defects: a) interstitial impurity atom, b)edge dislocation, c) self interstitial atom, d) vacancy, e) precipitate of impurity atoms, f) vacancy type dislocation loop, g) interstitial dislocation loop and h) substitutional impurity atom.

Due to the high lattice mismatch between GaN and used growth templates, different ways to reduce the interface tensions in epitaxial GaN layers have been developed [52–55]. The main themes are buffer layers, growth conditions and surface patterning. The best results have reduced the amount of dislocations down to 10^6 cm^{-2} in epitaxial GaN grown on foreign substrates [56]. Sapphire and silicon carbide substrates are commonly used in GaN epitaxy [57, 58]. Sapphire is relatively cheap but has a lattice mismatch of up to 22.7% depending on the crystal orientation [59].

More localized defects (point defects) are also often formed during epitaxial growth. For example, an atom can be missing from its designated position in the lattice (see figure 2.4d), generating a local discontinuity, called a vacancy

[45, 46, 60]. Further clustering of the point defects is also possible forming larger complexes [61]. A high concentration of point defects, or vacancies, can lead to poor optical performance [62]. Point defects (and dislocations) can be also introduced to the material after the growth via high-energy irradiation, which can remove, *e.g.*, a Ga atom from lattice site to interstitial site [63, 64].

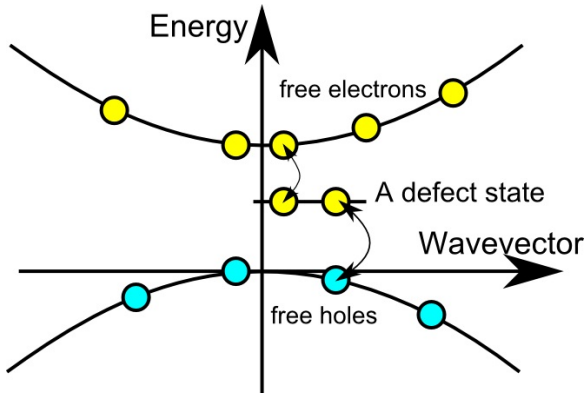

Figure 2.5. Illustration of recombination of the electrons and holes via a defect state inside the forbidden energy gap.

2.4 Vacancies

The two vacancy types for GaN are obviously gallium vacancy (V_{Ga}) and nitrogen vacancy (V_N) [65]. V_N is a quite typical native defect in GaN, acting as a donor, which can be seen as appearance of slight n-type conductivity in undoped GaN [45, 66]. V_{Ga} forms a deep acceptor state and has been associated with yellow luminescence (YL) in n-doped GaN [47, 46, 67–69]. However, some results are not in full agreement with this (see, *e.g.*, Publication V or Ref. 67). V_N is energetically more favorable in p-GaN than in n-GaN [45]. This is because the formation probabilities for vacancy defects depend on the Fermi-level position. Anyway, nitrogen vacancy is energetically more favorable over the whoe band gap compared to gallium vacancy [45]. The growth conditions affect the vacancy formation probability as well [45]. For example, nitrogen rich growth conditions favor formation of V_{Ga}. The vacancy formation energy (and formation probability) in general is dependent on the Fermi-level. Positron annihilation spectroscopy (PAS) measurements have indeed revealed much higher V_{Ga} concentration in n-GaN than in p-GaN [70, 67]. Thus, gallium vacancies are most likely present in important concentrations in MOVPE grown i- and n-GaN.

High energy electron beam induced V_{Ga} can be annealed out at temperatures above 500 - 600 K, with estimated migration energy of 1.5 eV. However, in-grown V_{Ga} in as-grown GaN has been observed to be stable up to 1300 - 1500 K temperatures. This has been associated with formation of complexes, possibly V_{Ga} - O [71]. Thus, it is likely that there is an important amount of V_{Ga} complexes in as-grown GaN n- and i-GaN.

2.5 Hydrogen-related complexes

Hydrogen is predicted to exist in GaN as H^+ and H^-. H^0 is unstable [72–74]. The migration barrier for H^- is large, 3.4 eV, but much smaller for H^+, 0.7 eV [72]. Solubility of H to n-GaN is much smaller than to p-GaN [74]. Due to its mobility, it is likely that hydrogen forms stable complexes in GaN when energetically favorable. Since hydrogen is present in large concentrations in typical epitaxial growth environments, *e.g.*, MOVPE, HVPE and ammonia-MBE, it is reasonable to expect hydrogen-defect complexes in GaN grown with these methods.

Hydrogen is expected to be strongly bonded to native defects where dangling nitrogen bonds exist [75]. This is indeed the case with gallium vacancies. Hydrogen can be bound to V_{Ga} as V_{Ga}-H, V_{Ga}-2H, V_{Ga}-3H and V_{Ga}-4H [76, 75]. The hydrogenated vacancies have lower formation energies than isolated V_{Ga}. Thus, these complexes are likely important in GaN. In p-GaN, hydrogen passivates the dominant acceptor Mg [77]. The formed Mg-H complex needs to be dissociated via post-treatment to obtain p-type conductivity.

2.6 Other complexes

For GaN, vacancy complexes such as, *e.g.*, V_{Ga} - C_N, V_{Ga} - (1-4)H, V_N - Mg and V_{Ga} - V_N, have been found [63]. These can contribute to different kinds of phenomena in GaN and related materials.

Related to the gallium vacancy, the V_{Ga} - O is interesting since it has a smaller formation energy than V_{Ga} alone. Thus, complex formation between Ga vacancies and substitutional oxygen donors is a likely process in GaN [78]. Divacancies, V_{Ga} - V_N, have much higher formation energy and are less likely [68]. V_{Ga} - O have also been associated with YL of GaN [68]. To completely

remove all oxygen contamination from epitaxial growth environment is virtually impossible, which explains the frequent oxygen related observations in GaN.

Another interesting complex is V_{Ga} - C. It has also been associated with the YL of GaN [79]. Obviously carbon is always present in MOVPE, where the metallic precursors are organic.

2.7 Doping

To be able to fabricate electronic devices, p- and n-type doping are needed. For GaN there are a few possible impurities that can be used in practical devices.

N-doping of GaN with silicon is quite straightforward. It can be easily achieved, *e.g.*, in MOVPE by introducing silane (SiH_4) to the growth environment. The dopant is active after growth and n-GaN resistivity is relatively low. Also oxygen can be used to obtain n-type conductivity in GaN, although Si is much more commonly used.

Obtaining p-type conductivity in GaN is more complicated. Mg is the only dopant that has been successfully used. Even so, as mentioned in section 2.5, Mg forms complexes with hydrogen leading to dopant passivation. This again leads to very high resistivity values. Thus, for Mg doped GaN, post-growth activation is necessary. Nowadays this is done by annealing the sample after the growth inside the reactor. However, post-treatment with LEEBI was formerly employed [80]. Thermal or LEEBI-activation significantly decreases the resistivity by breaking the Mg-H bond and activating the dopant.

Intrinsic (undoped) GaN has been observed to have a slightly n-type conductivity. This has been attributed to the V_N defects [42], as mentioned in section 2.4. Also impurities (*e.g.*, carbon) can play a role in unintended doping. Furthermore, different kinds of defect complexes can act as donors or acceptors [81].

3. Electron Beam - Gallium Nitride Interaction

This chapter describes the interaction between an e-beam and gallium nitride material.

3.1 Electron Energy Deposition

When an electron penetrates into a material, it can experience elastic or inelastic scattering when colliding with other particles. If the total kinetic energy of the atom-electron system is reduced in the collision, then the scattering is inelastic. (A part of the kinetic energy can be transfered to a photon, for example.) Otherwise it is elastic. In any case, momentum and energy are always conserved [82]. Scattered electron changes its trajectory and continues to traverse in the material as long as it still has kinetic energy left. The electron can scatter back to the direction if came from, and even escape the material. This backscattering can be utilized, for example, in SEM [83].

Inelastic scattering of electrons in the material can create so called secondary electrons, when the collision transfers sufficient energy from the primary electron to a bound electron to free it. The freed secondary electrons can again travel in the material experiencing collisions and hence freeing other electrons, resulting in an electron cascade. Thus, the secondary electrons contribute strongly to the energy spreading profile in the material.

Scattered electrons and secondary electrons can travel in any direction. Therefore, the area affected by electrons is much larger that just the beam spot size. For example, in EBL this creates the so called proximity effect, which means that the lines drawn by the e-beam will often be wider than intended. The scattering processes are illustrated in figure 3.1. A Monte Carlo simulation of an e-beam with 5 keV kinetic energy entering GaN from vacuum is shown

in figure 3.2. The simulation shows very clearly a path of an electron experiencing multiple collisions in the material. Also, some backscattered electrons, entering back to the vacuum, are visible.

As the electrons with sufficient kinetic energies can excite other electrons from atomic electron cores to higher energy levels, electrons can also recombine with the created empty states. The excess energy is then released, often as a photon. The emitted photon energy spectrum (typically in the X-ray range) is characteristic to the atomic electron core structure. This phenomenon is utilized, *e.g.*, in so called energy-dispersive X-ray spectroscopy (EDX) [84].

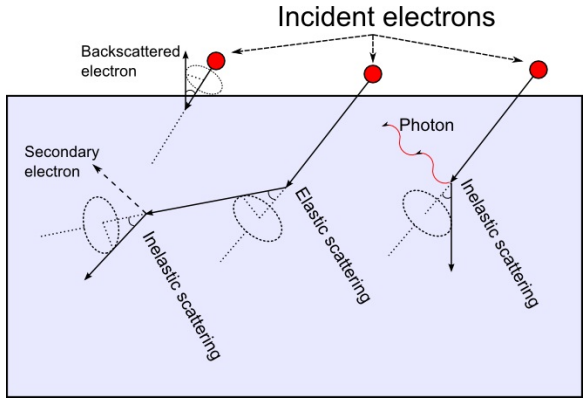

Figure 3.1. Illustration of electron scattering in material. Elastic, inelastic and backscattering are presented. The inelastic scattering creating both a secondary electron and a photon is presented.

Furthermore, the excess energy freed in the inelastic electron scattering can excite electrons from the valence band to the conduction band, thus creating electron-hole pairs. When the pairs recombine, the excess energy is emitted as photons, which have a spectrum corresponding to the material band structure, as discussed in section 2.2. This phenomenon is utilized in cathodoluminescence, described further in section 4.3.

Moreover, since electrons are charged particles, a dense e-beam can cause a local charged area in the material. Depending on the material conductivity and grounding, the total accumulated charge can be substantial. For example, sapphire and p-GaN are poor conductors, and are hence charged easily by the e-beam. This is easily demonstrated in SEM, when an electric field produced by the charging effects distorts the obtained image.

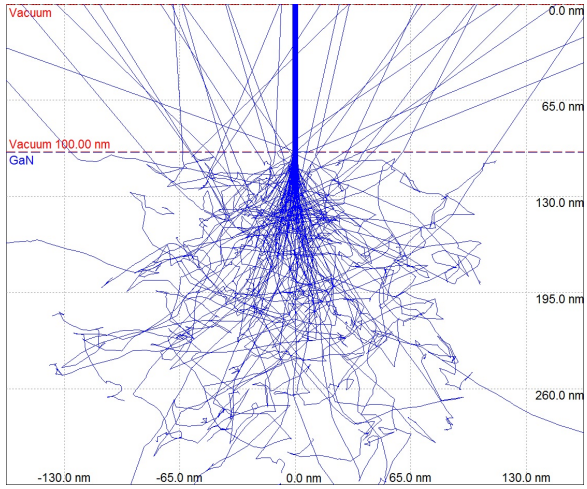

Figure 3.2. Monte Carlo 2D simulation of an electron beam with 5 keV energy and 2 nm radius, penetrating into GaN [85, 86]. The thick blue line in the vacuum center is the incoming beam and thin lines in the vacuum area are backscattered electrons. The number of displayed trajectories is 200.

3.2 Electron Beam Penetration

Calculations were performed to obtain the e-beam energy dissipation profile as it penetrates into the GaN lattice. This was done by using the cubic polynomial estimation of the Bethe-Bloch formula [87] describing the penetration profile [Publication II]. The Bethe-Bloch equation in cubic polynomial approximation form reads

$$\frac{dE}{dx} = \frac{fE}{R_G}(\alpha_0 + \alpha_1 y + \alpha_2 y^2 + \alpha_3 y^3), \tag{3.1}$$

where $R_G = kE^{1.75}\rho^{-1}$ is the so called Grün range, $k = 45.7$, ρ is the material density and f = 16.5 is the normalization coefficient. The parameters α_n were obtained from literature. From the results shown in figure 3.3, it can be seen that the energy dissipation with smaller energies happens sharply near the surface, but for higher energies the curve is broader and shifts deeper [87, 88].

Thus, the charge concentration in the material (charge per volume unit) is locally higher when the e-beam kinetic energy is small. For example, defect migration can be induced by electrostatic forces [62]. Therefore, it is possible that higher charge concentration could have an effect on the properties of GaN even if the kinetic energy of the beam is small. This is indeed true in, *e.g.*, Mg-doped GaN, where LEEBI has been used to activate the Mg-dopants, as

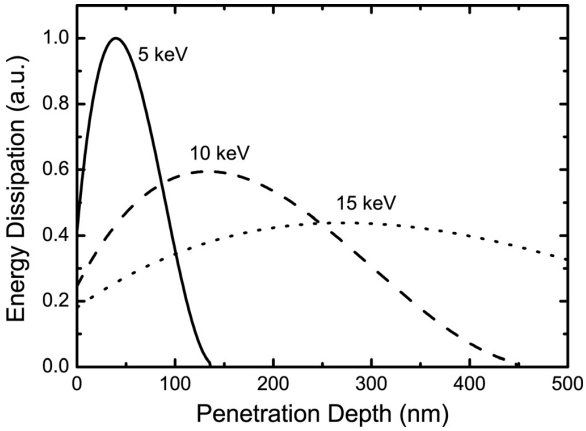

Figure 3.3. Energy dissipation curve for electrons in GaN. The curve for the lowest kinetic energy is clearly higher and located closer to the surface than those for larger kinetic energies [Publication I].

mentioned in section 2.7.

3.3 High Energy Electron Beam

The interaction of an e-beam and gallium nitride can be roughly divided in two parts: e-beam kinetic energies lower and higher than the minimum Frenkel pair formation energy. These energies are 150 keV for N-vacancy and 500 keV for Ga-vacancy, *i.e.*, a minimum of 150 keV of energy is needed to displace a nitrogen atom from the GaN lattice and a minimum of 500 keV is needed to displace a gallium atom. These energies can be obtained using the McKinley-Feshbach formula [89] with displacement threshold energies of 22 eV and 25 eV for Ga and N atoms in GaN, respectively [90, 66]. Thus, electron beam is considered to have high (kinetic) energy if it can create N- or Ga-vacancies (break the corresponding atomic bonds) and low (kinetic) energy if it cannot.

For example, TEM is a common tool utilizing electrons with kinetic energies above 100 keV. As the name suggests, the electrons are transmitted through the sample, experiencing absorption and scattering. The penetrated electrons can then be collected and analyzed to gain a very high resolution image (down to atomic scale) of the sample [91].

E-beams with high kinetic energies (*e.g.*, 2 MeV) have been used in defect studies for controllable defect formation. This way a sufficient amount of certain defects can be formed for extensive studies on their properties. Similarly, ions can be used to generate defects in the GaN lattice [92, 93].

3.4 Low Energy Electron Beam

In this work, the e-beam energies are well below the Frenkel-pair formation energy (*i.e.*, low energy e-beam) and therefore are insufficient to cause direct damage to the GaN lattice. However, the electrons can be absorbed to the material or they can scatter. The absorbed energy can either excite charge carriers or be manifested as heat. Low energy e-beam can hence be used in imaging (*e.g.* in SEM) or in lithography (*e.g.* in EBL). Furthermore, the flux of electrons will, of course, create a local area with negative charge. It is also possible for LEEBI to break weaker bonds (such as Mg-H) inside GaN (see section 2.7).

In this work, the e-beam has been characterized by its kinetic energy and the irradiation dose. The irradiation dose is defined as charge per area unit, absorbed by the material. Typical parameter range used in EBL is 5 - 30 keV for the kinetic energy and 0 - 200 μC/cm^2 for the irradiation dose. Within these parameters, the material heating should be negligible, as stated in Publication I.

4. Methods and Equipment

In this chapter, the fabrication and characterization methods used in this work are explained. The most important setups are discussed in more detail.

4.1 Metal-Organic Vapor Phase Epitaxy

Metal-organic vapor phase epitaxy (MOVPE) is a widely used epitaxial method to grow relatively good quality GaN (and other semiconductor) films and (hetero)structures [41, 94]. The metallic elements are introduced into the growth environment as metallo-organic compounds which then pyrolyze and release the metal atoms for growth. Nitrogen is usually introduced as ammonia (NH_3). The carrier gas can be either hydrogen or nitrogen. The temperature of the growth reactor is varied depending on the material and typically pressure of approximately 100 Torr is used. The released species react on the substrate surface, inheriting the lattice structure of the template, forming a crystalline film. The principle of the MOVPE method is shown in figure 4.1a and the chemical process is illustrated in figure 4.1b. With introduction of other elements, alloys like InGaN or AlGaN can be also grown. MOVPE has proven to be an effective tool in GaN-based light emitting device manufacturing.

The samples used in this study were grown on c-plane sapphire substrates by MOVPE. Ammonia (NH_3), trimethylindium (TMIn), and trimethylgallium (TMGa) were used as the N, In and Ga sources, respectively. First a 3-μm-thick undoped GaN buffer layer was grown on sapphire with the well-known two-step growth method [95]. For the GaN-film samples, a 3-micron-thick GaN layer was grown after the buffer layer. To grow the InGaN/GaN QW samples, a 3-nm-thick InGaN QW (emitting at 470 nm) was then grown on the GaN layer at 750 °C with an indium fraction of 12%. The QW was then covered by a GaN capping layer having a thickness of 10-40 nm.

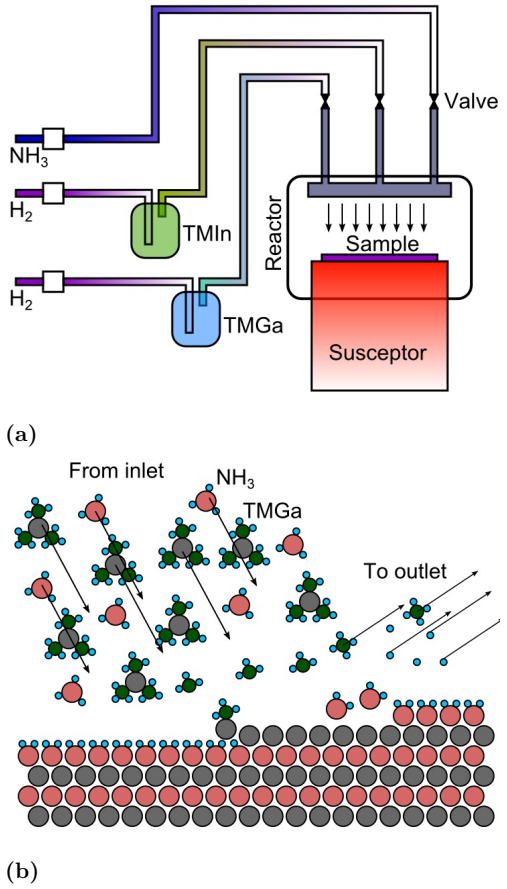

Figure 4.1. a) Illustration of a typical MOVPE system. b) Schematic of the MOVPE growth process.

4.2 Photoluminescence

In photoluminescence, light emission induced by electron-hole pair excitation by incident photons (discussed in section 2.2) is utilized. Typically, an intense laser beam is focused on the sample to create electron-hole pairs. When these electrons and holes recombine, the resulting photons are then collected and directed to a photo-sensitive detector. A filter can be used to select certain parts of interest from the spectrum or block unnecessary frequencies. The spectrum of the emitted photons is measured, giving information on the energy band structure of the material. PL measurement is non-destructive and a simple way to get information from the sample.

In this work, the PL spectra of the designated sample areas were measured at room temperature (RT) before and after the e-beam exposure using a

monochromatic He-Cd UV-laser ($\lambda = 325$ nm, I ≈ 80 W/cm^2) as an excitation source. The penetration depth of the laser beam into GaN is approximately 100 nm. The setup consisted of the excitation laser, a focusing lens (focal length ≈ 35 mm), a semi-transparent mirror, an optical fiber and a detector (Ocean Optics USB2000), shown in figure 4.2. The laser beam is focused on the sample, where it excites electron-hole pairs, which then recombine emitting light. The light is focused and directed to an optical fiber which leads the light to the detector. The detector used in this work can detect emission wavelengths between 200-1100 nm, with an accuracy of approximately 1 nm. The spectrum can then be recorded by a computer to store, analyze and display the data. The total PL intensity can be obtained by integrating the total area of the peak.

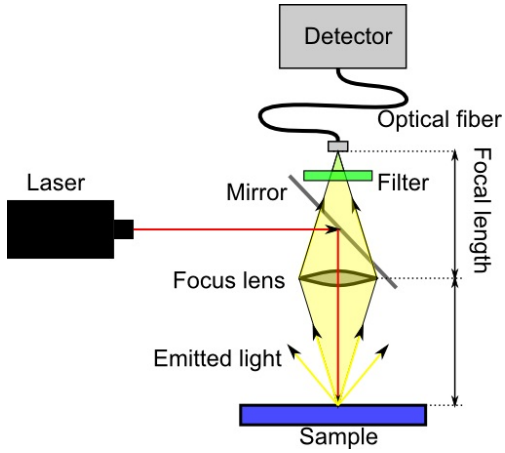

Figure 4.2. Schematic image of the PL setup used in this work. The red line represents the excitation laser beam and the yellow area represents the light emitted by the sample.

By measuring a reference point along with the treated points before and after LEEBI, the measured intensity of the irradiated points can be normalized using the reference PL. Hence, the contribution of possible fluctuations in the measurement setup can be effectively filtered out. The normalized PL intensities can then be compared between different samples with good accuracy. Of course, the original optical qualities and properties of the samples need to be approximately the same for the comparisons to be relevant.

4.3 Cathodoluminescence

In cathodoluminescence, an e-beam is directed to the material, *e.g.*, a semiconductor, under study. The impact of electrons with sufficient energy can trigger excitation - recombination processes of electron-hole pairs, which causes the sample to emit photons with certain spectrum, as discussed in section 2.2. Hence, CL is similar to PL (see section 4.2), with the exception that the electron-hole pair excitation is triggered by electrons instead of photons.

Due to the electron penetration profile into a material (see section 3.2), it is possible to obtain CL from different depths in the sample by varying the e-beam kinetic energy (*i.e.*, the acceleration voltage). This feature can be used for depth profiling. However, self-absorption of the material (*i.e.*, emitted photon is absorbed before it can escape) should also be taken into account since it alters the measured depth profile. Furthermore, due to scattering, CL is obtained from an area larger than the beam cross section.

In this work, the CL acceleration voltage was varied from 5 to 25 kV, the probe current was kept constant at 25 nA and the measurements were performed at room temperature. Obviously, CL is a method utilizing LEEBI, hence contributing to possible e-beam induced effects. However, in this work the luminescence did not change during CL measurement due to low total irradiation dose [Publication V].

4.4 Positron Annihilation Spectroscopy

Shortly described, in positron annihilation spectroscopy, positrons (anti-electrons) are accelerated and directed towards the specimen [96]. When a positron penetrates into the material, it can be trapped by certain kinds of defects in the lattice. This is because a suitable defect introduces a potential well for the positron to localize. After a time, positron-electron annihilation occurs and two gamma(γ)-photons are emitted (photon peak energy is roughly at 511 keV) to opposite directions. From the γ-radiation, the type and concentration of the possible defects can be determined. The measurements are based on positron lifetime in the material and the shape of the spectrum of the γ-photons created in the annihilation process.

The positrons are typically generated using a radioactive source such as ^{22}Na.

The emitted positrons have a wide kinetic energy spectrum with mean energies of hundreds of keV. Fast positrons can be directly used to probe bulk materials due to larger penetration depth. To study thin films, positrons need to be slowed down, typically to a few eV. This is done by using a moderator device composed of materials that have negative positron affinity (*e.g.*, most metals) [97, 98]. The slowed positrons can then be controlled with an acceleration voltage to get specific kinetic energies. Since the positron penetration profile (average penetration depth) is dependent on the positron kinetic energy, it is then possible to obtain measurement results as function of depth. The positron penetration profile is very similar to the electron penetration profile when both particles have the same kinetic energy, as can be seen in section 5.4 [Publication III].

Positron lifetime spectroscopy and Doppler broadening are the most commonly used measurements when utilizing positron annihilation. A positron entering a defect free crystal has an average lifetime, typical of the material, before annihilating with an electron. Furthermore, depending on the momentum of the electron, the annihilation produces a certain shape of the radiation spectrum. However, if there is a defect present in the crystal, the positron wave function can be localized, effectively trapping the positron. [98] When the positron gets trapped, the average lifetime before annihilation is altered. Also, annihilating electrons in the defect have different momentum values compared to electrons in a perfect lattice [98]. These changes produce lifetime and Doppler broadening values of the gamma spectrum typical for the defect.

In this work, the trapping of positrons at vacancy defects was observed as the narrowing of the Doppler-broadened 511 keV annihilation line, recorded with a Ge-detector. Typically, the shape change is characterized with two lineshape parameters, which can be obtained by comparing two different regimes of the perfect lattice spectrum and the defect altered spectrum. The parameters are usually denoted S and W, determined as fractions of positrons annihilating with low ($|p_L| < 0.4$ atomic units) and high momentum electrons (1.5 atomic units $< |p_L| <$ 3.9 atomic units), respectively [99]. p_L is the longitudinal momentum component of the electron-positron pair in the direction of the 511 keV annihilation photon emission. The difference can then be defined as the area between the curves at the peak (S) and the tail (W), as shown in figure 4.3a. From S and W parameters, the type and the concentration of the point defect can usually be determined [81, 67].

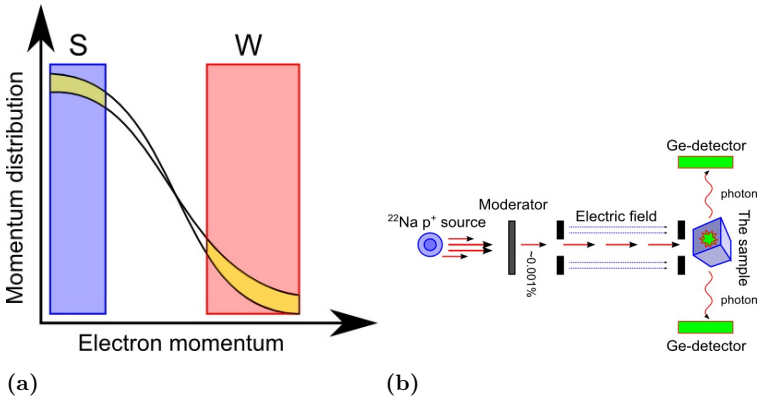

Figure 4.3. a) Illustration of obtaining the S and W parameters from the PAS measuremet. b) A simple schematic image of a typical PAS measurement setup. Typical moderator transmission is only 0.001% of (slow) positrons.

4.5 Scanning Electron Microscopy and Electron Beam Lithography

The resolution of conventional microscopes has a fundamental limit near the wavelength of the used light. Therefore, to study nano-scale specimens with radiation, a shorter wavelength is required. Scanning electron microscopy utilizes a well focused low energy e-beam accelerated towards the sample surface. The beam is scattered from the sample and received by a detector (see figure 4.4). From the position of the beam and from the intensity of backscattered electrons, an image can be constructed. SEM is capable to obtain a resolution of just a few nanometers, depending mostly on the beam focus spot size. Furthermore, the e-beam can be utilized, *e.g.*, in electron beam lithography, to create nano-scale patterns on the sample. In this work, EBL was used for patterning of silver nano-gratings on InGaN QW sample surface. Since the e-beam can be focused to a spot of only few nanometers, the resolution of the drawn pattern can be very high.

In EBL mode, the e-beam draws a pre-defined pattern on a certain position. In SEM mode, a large area of the surface is irradiated by rapidly sweeping the focused beam on the surface and the back-scattered electrons are used to determine the surface structure. There are no differences in the beam itself, only in the sweep pattern. Therefore, SEM can be used to irradiate large areas of the sample without the need for defined patterns.

The key parameters in (any) LEEBI application are the acceleration voltage (and corresponding electron kinetic energy), the beam current, the exposure

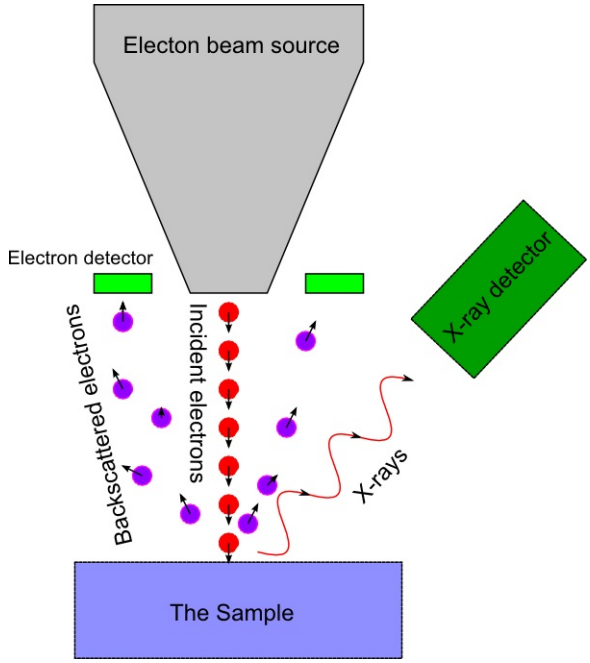

Figure 4.4. Illustration of a SEM setup. Additionally an x-ray detector is presented illustrating an EDX setup.

time and the exposed surface area. Typically, acceleration voltages of 20 - 50 keV are used. The surface area of an irradiated spot equals approximately the beam cross section. The electron scattering and secondary electrons spread the actual irradiated area to some degree. The beam spot size hence roughly defines the minimum line width of the pattern together with the used resist material. The necessary current and exposure time are together defined as the exposure dose given as $D = t \times I/A$, where t is the exposure time, I is the incident beam current and A is the irradiated area. Typically the resist material is chemically altered when a high enough dose is applied. For example, for 100-nm-thick (poly)methyl methacrylate (PMMA), the needed dose is around 100 μAs/cm^2.

In this work, the samples were exposed to an e-beam using a Zeiss Supra 40 SEM. The LEEBI exposure was performed by rapidly sweeping the e-beam on a specific area of the sample surface (SEM mode). The e-beam energy was varied between 5 and 20 keV and the dose in the range of 0−508 μC/cm^2 (0−3×10^{15} cm^{-2}) by controlling the exposure time and the beam current. For the EBL patterned samples, the e-beam energy was 20 keV and the dose typically 70−120 μC/cm^2 depending on the line width. The e-beam spot size was approximately 2 nm in diameter and the corresponding momentary

current density was 0−100 kA/cm^2.

5. Low Energy Electron Beam Irradiation Effects on GaN

In this chapter, the main results of this work regarding the LEEBI effects on GaN are presented and discussed.

5.1 InGaN/GaN QW Degradation

The origins of our investigation to the LEEBI induced optical degradation are in fabrication of silver nano-grating patterns. The goal was to gain an increase in light extraction from a QW structure, utilizing plasmonic coupling to more efficiently inject the generated photons to air. (This is presented in more detail in chapter 6.) The patterns were made using a SEM/EBL tool described in section 4.5. For this reason, silver nano-gratings were fabricated on samples with near surface InGaN/GaN QW (λ = 475 nm) capped with 10-40 nm of GaN. PL intensity increase was indeed successfully found as shown in Publication VI. However, while conducting the PL measurements, an unexpected reduction in luminescence intensity was observed on the sample area exposed to LEEBI but left without metal. This discovery yielded the need to gain more insight on how the LEEBI might affect the luminescence of GaN-based samples, since any reduction in the emission efficiency would decrease the enhancement factor.

The samples used for the original extraction enhancement trials were first considered to be sensitive to the e-beam due to the InGaN active layer near the surface. Due to the degraded PL intensity, it was reasonable to assume that the QW had been damaged. Thus, samples with different QW depths (*i.e.*, capping layer thickness) were fabricated to study both dose and penetration dependence of the LEEBI induced damage. The samples were exposed to different LEEBI doses (charge / surface area unit) and kinetic energies.

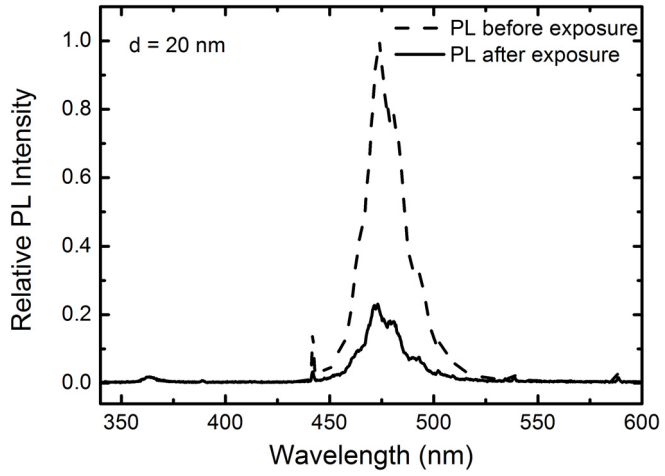

(a)

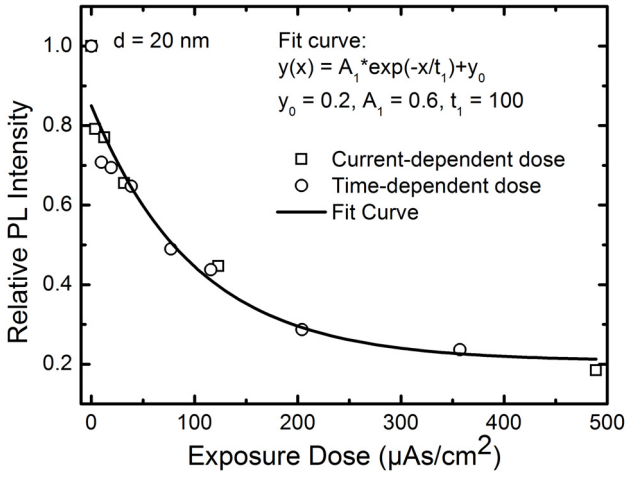

(b)

Figure 5.1. a) Example of damaged (full line) and undamaged (dashed line) InGaN SQW spectra. The capping layer thickness (d) was 20 nm. b) InGaN SQW normalized PL intensity as a function of 20 keV e-beam irradiation dose [Publication I].

As shown in figure 5.1, the PL intensity experiences a dramatic drop after LEEBI [Publication I]. The reduction of PL as a function of the exposure dose appears to have an exponential dependence. However, the exponential fit in the picture is mainly meant as a guide for the eye. It can also be seen from figure 5.1b, that the increasing dose realized by either increasing exposure time or beam current produces the same effect.

Interestingly, as shown in figure 5.2, the PL degradation is larger for smaller e-beam kinetic energies. This was surprising, since it was originally assumed

that the kinetic energy is responsible for the damage. The damage to the PL is much more severe using, *e.g.*, 5 keV kinetic energy instead of 10 keV, and the difference between 10 keV and 15 keV induced damage is smaller. This can be explained with the e-beam energy dissipation profile shown in figure 3.3. With smaller kinetic energy, the beam dissipates in a much smaller volume, thus affecting it more intensely.

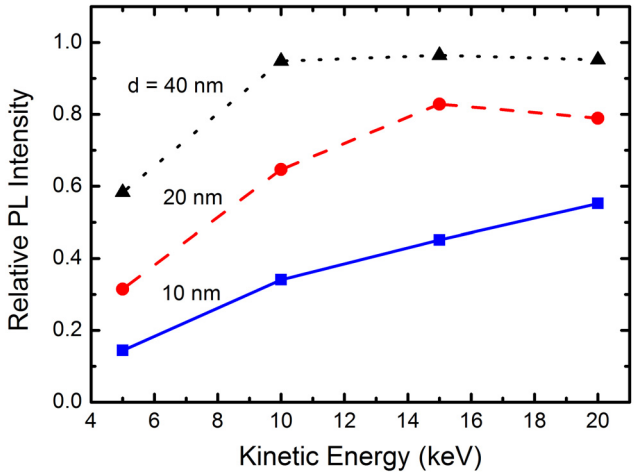

Figure 5.2. InGaN QW PL intensity as a function of the e-beam kinetic energy for three different capping layer thicknesses [Publication I].

Moreover, as shown in figure 5.2, the PL degradation was observed to be smaller with a thicker capping layer, meaning that thicker capping layer should protect the QW better. It was observed, some time after Publication I was released, that this is not in perfect agreement with the calculated energy dissipation profile in GaN (see section 3.2). The curve for, *e.g.*, 5 keV beam in figure 3.3 predicts the maximum energy dissipation to the depth of approximately 50 nm. Therefore, e-beam penetration to InGaN/GaN QW structure was simulated using the Casino simulation program [85, 86]. The results are shown in figure 5.3. It can be seen that the absorbed energy has a maximum very close to the first quantum well (QW 1) and then decreases rapidly before the next QW position. The simulation was also done on pure GaN film without the QWs, which showed that the thin InGaN layer effect to the energy profile is negligible. Thus, the simulation data is in very good agreement with the results in figure 5.2. This also suggests, that the parameters for the Bethe-Bloch cubic approximation calculations might need to be corrected to produce a sharper peak closer to the surface. Nevertheless, the calculated curves in figure 3.3 are a good approximation to the nature of the degradation as a function of the beam kinetic energy.

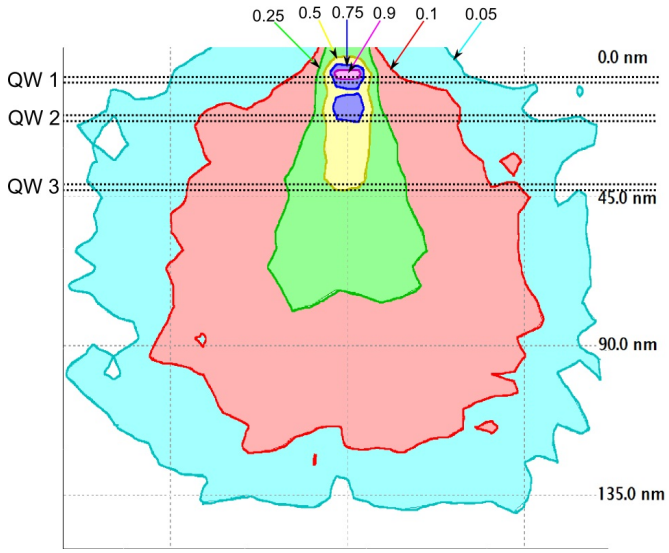

Figure 5.3. Simulated absorbed energy of an of electron beam (radius 2 nm, kinetic energy 5 keV) in GaN with three embedded InGaN QWs. The wells are 3 nm thick and located at the depth of 10, 20 and 40 nm for QW 1, QW 2 and QW 3, respectively. The maximum energy is located at the depth of QW 1. The result is the same with or without the QWs.

Hydrocarbon contamination, induced by LEEBI, has been reported earlier on sample surfaces [100]. Hence it was deemed possible that the contamination might cause some PL degradation, even if the observed smaller degradation with thicker capping layer already did not support this. To be sure, InGaN samples were fabricated and irradiated heavily with an e-beam. The resulting contamination was indeed visible in SEM as dark lines. The dark lines were easily removed with acid treatmets (3:1 H_2SO_4:H_2O_2 and 1:3 HNO_3:HCl). However, the PL, observed to be degraded from the prior LEEBI, was not recovered [Publication II]. Thus, the hydrocarbon contamination was excluded as a source of reduced luminescence.

To investigate the dependence between the In fraction and the degradation, QW samples with two different In content were fabricated. GaN / $In_xGa_{1-x}N$ / GaN near-surface samples with x = 0, x = 0.12 and x = 0.20 were grown. Obviously, x = 0 case is identical to GaN film with no QW. The samples were exposed to 10 keV LEEBI with varying doses. The results are shown in figure 5.4. It can be seen, that the PL intensity degradation for both QW samples is almost identical. This points to a conclusion that optical degradation of the QW is not dependent on the indium fraction. However, the band-edge emission intensity of the GaN film degraded slightly more than those of the QW. Thus, more careful investigation of pure GaN films was started.

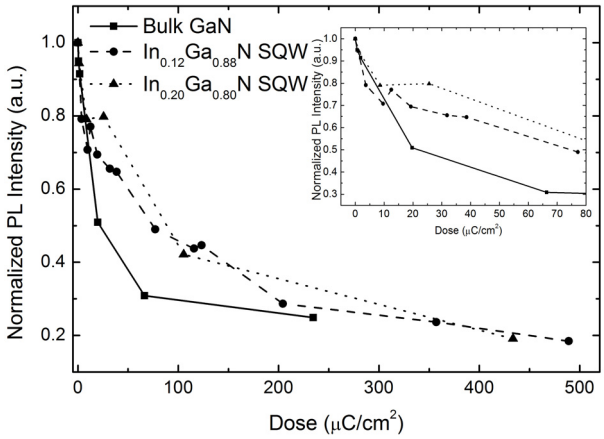

Figure 5.4. $In_xGa_{1-x}N$ QW PL intensity as a function of LEEBI dose for x = 0, x = 0.12 and x = 0.20 indium fractions. Inset gives a closer view of the 0 - 100 $\mu C/cm^2$ region. Improved image of [Publication II].

If the optical degradation of the QW luminescence was related to changes in the In content or distribution, or to dislocation glide (which have both been reported in case of transmission electron microscopy (TEM) using higher e-beam energies [101, 102]), then some change should also be noticed in the peak position and/or FWHM of the PL spectra. In fluctuations and dislocations both change the QW band properties. However, this was shown not to be the case: both peak position and FWHM were observed to remain unaltered (within the measurement resolution < 1 nm) after the LEEBI even with a dramatic damage to the PL intensity. Thus, changes in the QW indium composition and dislocation density became an unlikely candidate for the damage mechanism.

5.2 MOVPE GaN PL Degradation

The next logical assumption for the damage mechanism involves the investigation of the barrier material surrounding the QW, namely undoped GaN. Thus, the same LEEBI experiments were performed on MOVPE-grown GaN films as previously for the InGaN/GaN QW.

The results show (figure 5.5) that the BE luminescence of MOVPE grown GaN is degraded, when exposed to LEEBI. This was surprising in the sense that GaN is usually considered to be highly resistant to radiation. The kinetic energy of the e-beam should not be sufficient to break any chemical bonds of

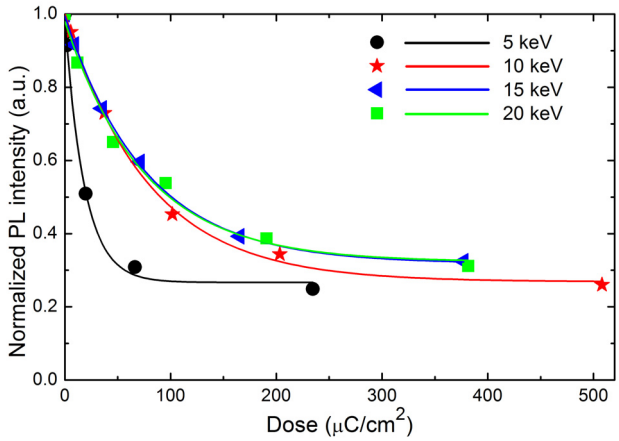

Figure 5.5. PL intensity as a function of irradiation dose for GaN samples irradiated with 5 - 15 keV energies. The higher impact of smaller kinetic energy is clearly observable [Publication III].

the GaN lattice. The degradation as a function of the exposure dose shows the same exponential behavior as in the case of the InGaN/GaN QW sample. Furthermore, the degradation as a function of the kinetic energy also behaves as in the case of the QWs: the lower kinetic energy induces more damage. Also, as in the QW samples, the peak position and FWHM of the band-edge luminescence spectra (see figure 5.6) remained unaltered, even when measured in 20 K with a highly accurate ($\Delta\lambda = 0.1$ nm) monochromator.

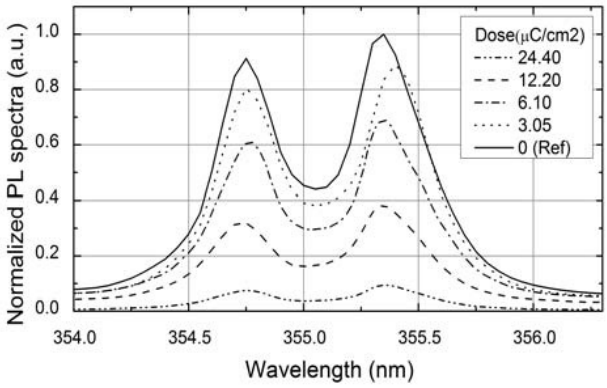

Figure 5.6. The normalized PL spectra of an irradiated GaN sample, measured in 20 K, showing that the FWHM and the peak position remain unaltered [Publication II]. Free exciton (354.75 nm) and bound exciton (355.30 nm) peaks can be distinguished.

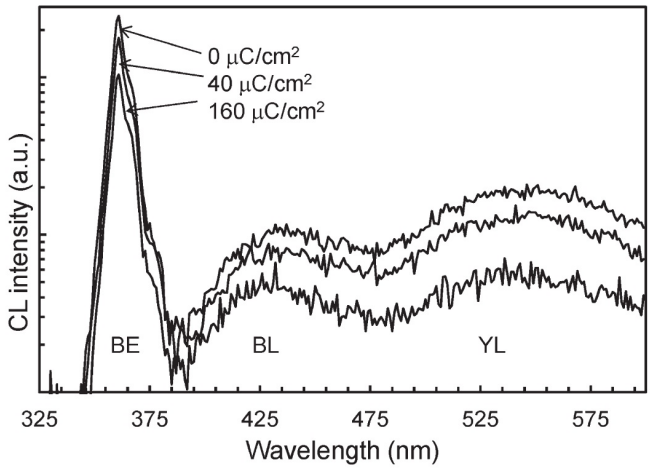

Figure 5.7. CL spectra for three different exposure doses. The CL intensity axis is logarithmic. The coincidental YL and BL degradations are clearly visible [Publication V].

5.3 MOVPE GaN CL Degradation

To support the PL measurements, cathodoluminescence was used to verify the LEEBI induced degradation [Publication V]. The samples were first irradiated with the LEEBI tool and then measured with the CL equipment. In this case, the CL probe irradiation dose was too small to cause further degradation to the samples, as indicated in Publication V. Luminescence intensity degradation was (figure 5.7), in good agreement with the PL measurements. As seen in figure 5.8, the largest amount of damage is observed with 5 kV CL acceleration voltage. This is to be expected since CL energy closer to 5 kV probes the volume affected by the 5 keV LEEBI more accurately. The CL spectra (figure 5.7) also show, that the yellow and blue band (BL) luminescence degrade as a function of LEEBI dose. This indicates, that the involved degradation mechanism produces non-radiative recombination centers to the material.

In fact, degradation of GaN-based optical devices, such as laser diodes, operating under high current densities, has been reported in the past [103, 104]. The degradation mechanism in these devices, just as in the samples used in this work, could involve generation of non-radiative recombination paths. These paths are mainly linked to defects in the semiconductor lattice. Thus, investigation of possible defect generation during LEEBI was initiated.

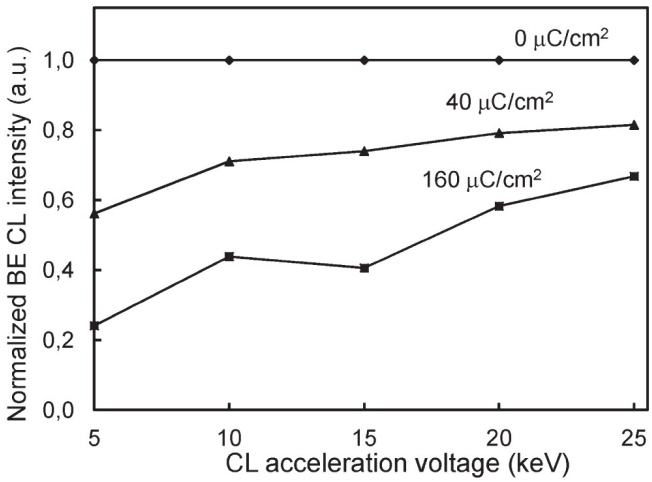

Figure 5.8. CL band-edge luminescence intensity as a function the CL acceleration voltage for three different exposure doses (0, 40 and 160 μC/cm^2) made by 5 keV LEEBI. The larger measured degradation with smaller acceleration voltage is clearly observable [Publication V].

5.4 Point Defect Appearance

At this stage of the investigations, it was known that the PL degradation was due to changes in the GaN films in general, and that there was probably a non-radiative recombination mechanism present after LEEBI. Hence, it was reasonable to try to find defects in the lattice, appearing after the irradiation, that could be the cause of the damage. Since newly generated dislocations were already ruled improbable (see section 5.3), positron annihilation spectroscopy was used to find out the possible changes in the point defect concentrations in the samples. Point defects as the source for non-radiative recombination has been proposed before [105]. Since positrons have basically the same depth profile in GaN as electrons (see figure 5.9), they effectively scan the same volume that has been exposed to the e-beam.

The measurement showed (figure 5.10) a clear increase in the PAS S parameter (explained in section 4.4) with increasing LEEBI dose. The S parameter is known to be related to the amount of point defects in the material [81]. Furthermore, it can be clearly seen that the increasing S parameter and decreasing PL intensity have a high anti-correlation to each other. Thus, it was shown that the detected point defect concentration of GaN increases under LEEBI. In figure 5.10, the S parameter saturates to a value of approximately 0.4485, which corresponds to point defect concentration of about 2×10^{17} cm^{-3} [99].

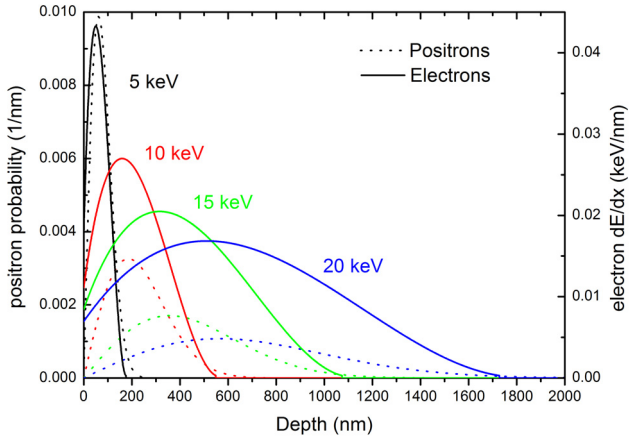

Figure 5.9. Energy dissipation curves of electrons and positrons in GaN. The depth profile is observed to be very similar [Publication III].

For reference, the point defect concentration on non-irradiated sample area is below the PAS RT detection limit of about 1×10^{16} cm^{-3}, typical for MOVPE GaN [70].

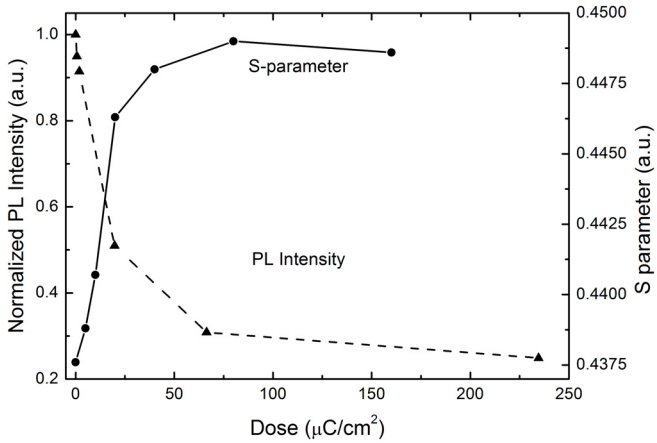

Figure 5.10. PAS S parameter and the PL intensity as a function of the LEEBI dose. A clear anti-correlation can be seen [Publication IV].

5.5 In-Grown Gallium Vacancies

The PAS measurement data gives further information about the nature of the defects in the material. By plotting both W and S parameter, it is possible to identify different kinds of point defects [81, 67]. The results clearly show (figure 5.11), that with increasing LEEBI dose, the PAS result evolves along

the line typical for V_{Ga}. Furthermore, the gallium vacancies can be also observed to have the signature of an in-grown vacancy, rather than one created by high energy e-beam irradiation after growth [70, 67]. The difference is distinguishable most probably because of the impurities present in the in-grown vacancies. However, when V_{Ga} is created by radiation after the growth, it is pure with no impurity atoms present. The positron lifetime and system momentum are usually measurably altered when the vacancy is complexed or clustered.

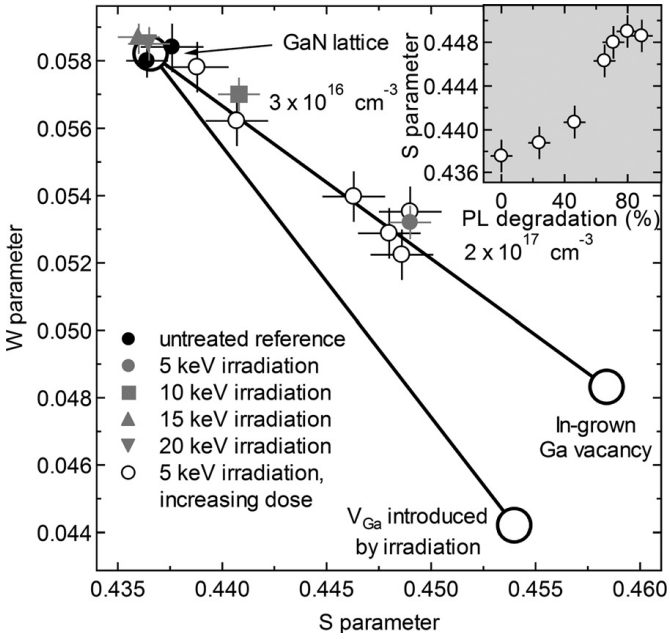

Figure 5.11. PAS S parameter and W parameter plot. The dark line serves as an indicator to point the vacancy type. The inset shows the S parameter as a function of the PL intensity degradation [Publication III].

Judging from the previous, the gallium vacancies observed here must be created during growth in the MOVPE reactor. Thus, the assumption of (ideal) GaN having good radiation resistance is valid, but some sensitivity can arise from certain kinds of in-grown defects. As discussed in Publication III, since the GaN PL intensity is degraded with the increase in the observed concentration of V_{Ga}, it can be concluded that these gallium vacancies are invisible to the PAS measurement before LEEBI, *i.e.*, V_{Ga} have been passivated by some mechanism.

5.6 Hydrogen Passivated Gallium Vacancies

The best candidate to explain the passivation of the gallium vacancy prior to LEEBI seems to be hydrogen. It is likely in MOVPE GaN that the V_{Ga} are complexed with H-atoms (V_{Ga} − (1-4)H) [81]. However, 1H- and 2H-complexes are visible to PAS and the 4H-complex is unstable. Furthermore, 3H-complexes have been shown to be neutral through the band gap and to be invisible to PAS [75]. The removal energy of hydrogen from V_{Ga} − 3H is Fermi-level dependent but in the range of 1 eV. Moreover, as mentioned in section 5.5, the signature of in-grown V_{Ga} in PAS S - W plot is probably due to impurities associated with the vacancy. For these reasons, we propose that MOVPE grown GaN contains a significant amount of in-grown V_{Ga}, that are passivated by 3H-hydrogen complex, and can be activated by LEEBI. The situation seems to be similar to the activation of Mg dopants with e-beam irradiation (see section 2.7).

Our results do not directly support the literature claims, that V_{Ga} would be responsible for the GaN YL. This is due to the CL spectra (see section 5.3) where the YL and BL degrade along with the band-edge luminescence. However, the YL has also been attributed with different defects, *e.g.*, V_{Ga} - O, V_{Ga} - C and V_N. In general, the relation between V_{Ga} and YL (and BL) is not clear. [106, 62]

5.7 Recovery by Thermal Annealing

If hydrogen passivation is the reason for the in-grown V_{Ga} to be undetectable prior to the LEEBI, it is reasonable to see if sample annealing could be used to re-passivate the vacancies. Both V_{Ga} and H are known to be mobile in elevated temperatures (see secs. 2.5 and 2.4). Thus, 500 ° C annealing up to 52 h was performed on samples irradiated with a 5 keV e-beam with doses of 0 - 180 μC/cm^2.

The results of the annealing experiment are shown in figure 5.12. It can be seen that the PL intensity indeed recovers partially after relatively short time ($<$ 60 sec) of annealing. However, longer annealing did not recover the PL to the original state, but the recovery saturation was very fast. From highly degraded sample (20% of the original PL) the recovery was approximately to 50% of the original PL intensity.

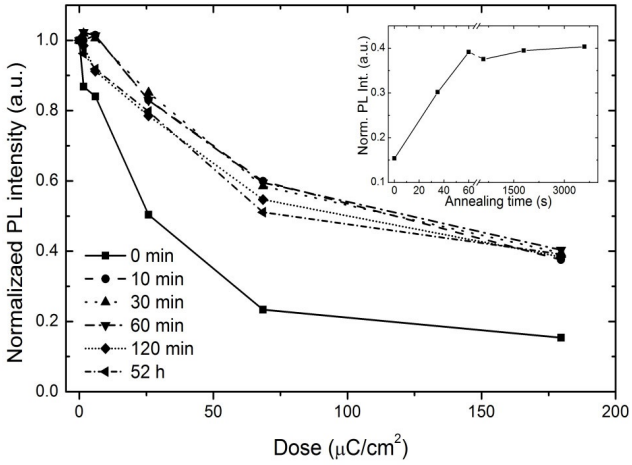

Figure 5.12. Recovery of the PL intensity by annealing at 500 ° C. The inset shows the normalized PL values as a function of annealing time (LEEBI dose 180 μC/cm^2) [Publication IV]. The value of each measurement point has been normalized to that of the untreated sample, sometimes causing the value to exceed unity.

The possible contribution of the annealing ambient to the recovery of the PL intensity was also studied. Two samples were first irradiated with 5 keV e-beam to create significant amount of PL intensity degradation and then one sample was annealed in H_2 and other in N_2. As can be seen from figure 5.13, the annealing ambient (H_2 or N_2) did not have significant effect on the PL recovery.

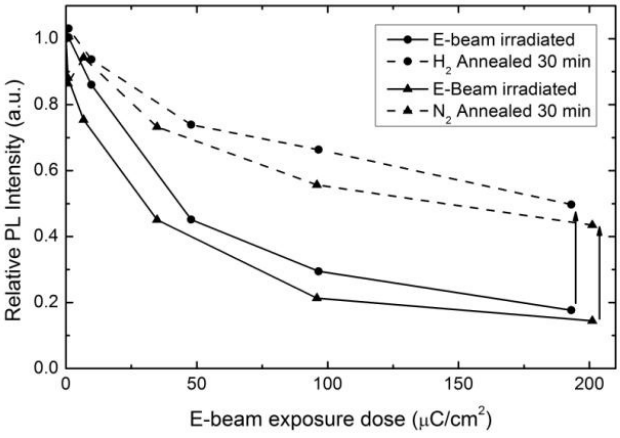

Figure 5.13. PL intensity as a function of e-beam exposure dose for two GaN samples: first irradiated with 5 keV e-beam (solid lines) and then annealed 500 ° C 30 min in H_2 and N_2 (dashed lines) [Publication IV]. The value of each measurement point has been normalized to that of the untreated sample, sometimes causing the value to exceed unity.

The current assumption is that due to relatively poor solubility of H to GaN

(see section 2.5), the hydrogen ambient cannot contribute to the re-passivation of V_{Ga}. However, the hydrogen already present in GaN can migrate (back) to the V_{Ga} sites. Of course, part of the hydrogen might diffuse out of the sample or otherwise be unreachable by the vacancies, thus explaining why the recovery is not total.

5.8 Comparison of H_2 and N_2 Carrier Gases

The sources of hydrogen, especially in MOVPE grown GaN can be many. Ammonia breaks down in the reactor freeing nitrogen for the growth process. As a result, also hydrogen is generated. Furthermore, the metal precursors trimethylindium and trimethylgallium contain hydrogen and trace amounts of, *e.g.*, water and other contamination sources can be present. Finally, H_2 is often used as a carrier gas for the precursors.

The contribution of the carrier gas as a hydrogen source is straightforward to investigate: two i-GaN samples were grown, one with H_2 and one with N_2 carrier gas. LEEBI exposure was performed on them with similar parameters: 5 keV energy and approximately 0 - 200 $\mu C/cm^2$ dose. The PL intensity was measured from both samples. The results are seen in figure 5.14.

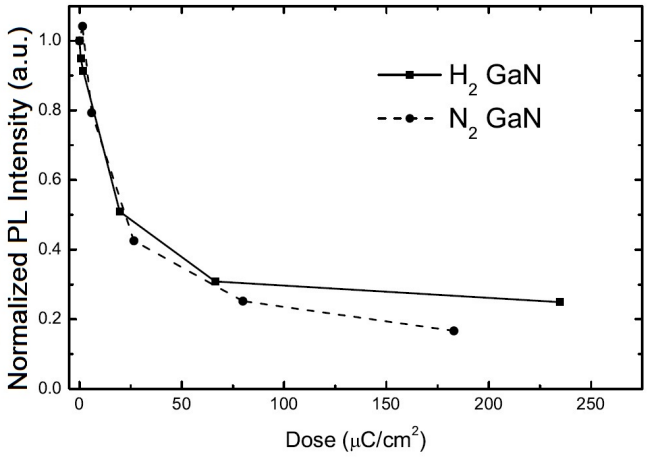

Figure 5.14. Recovery of the PL intensity by annealing at 500 ° C. The inset shows the normalized PL values as a function of annealing time [Publication IV]. The value of each measurement point has been normalized to that of the untreated sample, sometimes causing the value to exceed unity.

It can be clearly seen that the two curves are very similar. No clear difference is present in the PL degradation. This strongly indicates that the carrier gas does not have any significant impact on the formation of the V_{Ga} - H (or

other possible) complexes that contribute to the optical degradation. Since the measured vacancy concentration is low compared to concentrations of Ga and N, and since hydrogen is quite mobile in GaN (especially at high temperatures), even a small amount of H could passivate the gallium vacancies quite efficiently.

6. Enhancement of Luminescence by Nano-Gratings

This chapter describes the results of the study of GaN/InGaN/GaN near-surface QW luminescence enhancement using silver nano-gratings.

6.1 Motivation

A modern GaN-based light emitting device can achieve very high internal efficiency, well above 50% [107, 108]. (This means that inside the device, more than 50% of the recombinations of the injected carriers emit light.) Unfortunately, there are factors limiting the total external efficiency of these devices. In GaN-based light emitting devices, the total internal reflection is the main extraction limiting factor. Due to the large difference between the refractive indices of air ($n \approx 1$) and GaN ($n \approx 2.3$), only less than 4% of light created in the device active region can escape through a flat surface (assuming the possible extraction from the sides is not included) and the rest is lost. This is illustrated in figure 6.1. For this reason, solutions for enhancing the extraction efficiency of these devices are needed.

The most commonly used method to improve extraction is the epoxy encapsulation. The flat LED surface is covered with a dome of transparent material with refractive index higher than air (*e.g.*, $n = 1.50$). This increases the critical angle, thus increasing the extraction. The best materials can yield up to 4-fold enhancement. Unfortunately, at the moment this is the maximum achievable enhancement using practical epoxy materials.

The layers of the light emitting device structure act as waveguides for light, *i.e.*, the (trapped) light propagates in the material [109, 110]. The propagating modes present in the layers depend on the layer dimensions and material properties. One approach to enhance the extraction efficiency is to scatter

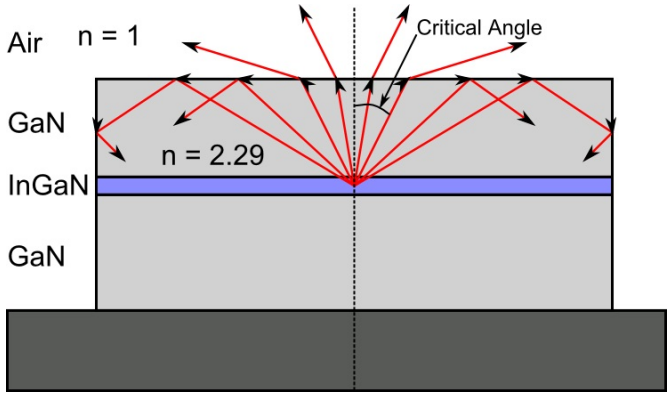

Figure 6.1. Illustration of light extraction from a LED structure with planar surface. Only light emitted below the critical angle can escape, seriously limiting the device efficiency.

these waveguide modes using surface roughening. In practice, this can be done, *e.g.*, by growing on a patterned substrate or with post-growth treatment such as etching [111–113]. Up to 3-fold improvement can be achieved in extraction. However, engraving of the GaN surface is often difficult due to chemical and mechanical hardness. It can also require expensive lithography.

Plasmonic coupling has been used to enhance light extraction up to 5-fold [114]. Thus, this technique is potentially very effective. The problem is that the light emitting region must be very close to the plasmonic metal interface due to the fast exponential decay of the plasmon wave in the direction perpendicular to the surface. This creates great difficulties especially in creating electrically pumped devices, since the metal too close to the active region will disturb the normal operation of the device. Hence, it is not possible to find a suitable distance between the grating and the active region in the conventional LED design.

6.2 Grating Structure

The plasmonic coupling effect has yielded very large enhancement of the light extraction in literature. Thus, the goal in this work was to create a periodic metal structure capable of first capturing photons from the device active region to plasmonic modes, and then re-emitting the them as photons outside the structure. As mentioned before, the active region (the QW) must be very close to the metallic interface. For this reason, near-surface InGaN QW (λ = 475 nm) samples were grown (using MOVPE), having only 20-nm-thick

GaN capping layer on top of the QW. According to calculations, this distance should be sufficient for the plasmonic coupling. The excitation of this kind of structure can be effectively done with a laser beam from behind the device.

Silver was selected as the interface material since it is good conductor of plasmonic waves and electron beam sputtering and EBL patterning of Ag is relatively easy. A schematic of the structure is shown in figure 6.2a and a SEM image of a real fabricated silver nano-pattern is show in figure 6.2b. Based on early calculations, the metal thickness of 35 nm was selected and the periodicity between 200 and 250 nm (*i.e.*, the gap between silver lines is constant 100 nm and the silver stripe width varies between 100 and 150 nm). The largest challenge in the fabrication of the silver grating is created by the relatively poor conductivity of the GaN surface. The surface charging of the resist polymer and GaN is large since the injected electrons cannot escape very quickly. The charging generates electric fields that can interrupt the direct path of the e-beam, distorting the drawn image. This problem was circumvented by using smaller beam current and larger exposure time and high enough acceleration voltage.

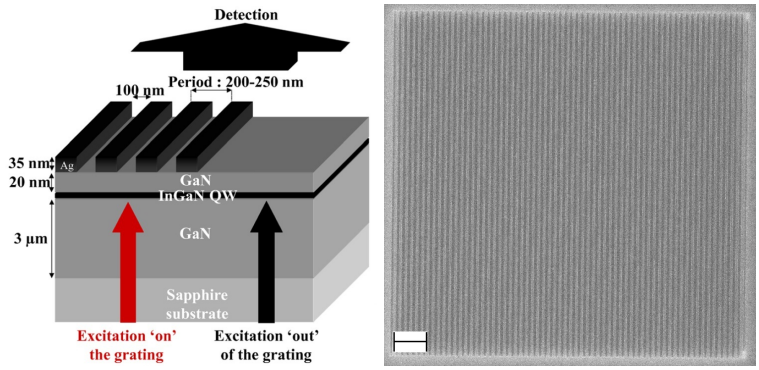

Figure 6.2. a) Schematic of the fabricated silver nano-grating structure on top of GaN/InGaN/GaN QW [Publication VI]. b) SEM image of a fabricated silver grating. The scale bar corresponds to 2 μm.

In addition to the silver grating, part of the samples were coated with a thin polyvinyl alcohol (PVA) layer. This changes the plasmonic and waveguide behavior of the structure. Thus, the samples with and without the PVA layer can be compared and the possible differences analyzed.

6.3 Luminescence Enhancement

As can be seen from figure 6.3c and d, the measured luminescence is significantly enhanced with silver grating and PVA on top of the QW. The measured total PL intensity has increased to approximately 2.8-fold, compared to a flat surface emitter. Especially, the TE polarized extraction is enhanced (figure 6.3c). There is no extraction enhancement with the PMMA grating (figure 6.3a) and only very small enhancement with the silver grating having no PVA layer on top (figure 6.3b).

The smaller enhancement of the TM mode light was slightly surprising since the plasmon related waves should be TM polarized. Using simulations together with angle resolved PL measurements and reflectometry measurements, it was found out that the improvement in the extraction was actually not caused by plasmonic coupling. The silver grating was seen to be able to diffract light out from the guided modes of light propagating in the GaN and PVA layers, in the same manner as in structures with roughened surface. The details of the measurements and simulations can be found in Publication VI. The smaller enhancement of the TM mode could then probably be explained with the larges losses related to the plasmonic waves that are created but not emitting the light out. The need for the PVA layer to gain any significant enhancement is related to the creation of a waveguide on top of the grating. The metal needs to be buried between two waveguides to have high enough strength of the optical field at the grating interface.

It can be concluded that a silver nano-grating buried in PVA can significantly increase the light extraction from a GaN-based light emitting device. The enhancement is based on diffraction of waveguide modes from the device layers in a similar manner to the surface roughening technique. Further optimization of the structure can probably yield a significantly higher extraction enhancement. The LEEBI induced GaN optical degradation (discussed in chapter 5), is most likely also present in these devices. Thus, optimizing the EBL process with regard to the degradation (*e.g.*, utilizing higher bean kinetic energy, smaller exposure dose or protective layers), or substituting EBL with another lithography process, should further improve the excitation. However, the current 3-fold enhancement is already at the same level with the conventional surface roughening and epoxy encapsulation. Furthermore, the structure could be further optimized to utilize the plasmon related enhancement.

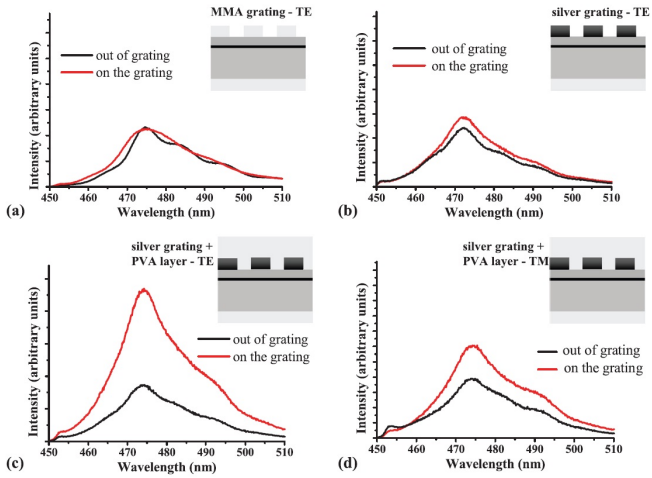

Figure 6.3. Spectra of the patterned and reference samples with: a) PMMA polymer pattern, TE-polarization b) silver nano-grating, TE-polarization c) silver nano-grating and PVA layer, TE-polarization d) silver nano-grating and PVA layer, TM-polarization [Publication VI].

7. Summary

In this thesis, the influence of LEEBI on GaN and InGaN has been studied. The results clearly show optical degradation of the materials, namely reduction in BE emission intensity, after sufficient LEEBI exposure. The damage to the optical quality has been shown to be as high as 85% in the studied parameter range. The mechanism of the degradation is suggested to involve activation of point defects in the GaN lattice. These point defects have been identified as in-grown V_{Ga}, that can act as unwanted recombination sites for the charge carriers. The activation mechanism has been hypothesized to involve a LEEBI induced removal of hydrogen from $V_{Ga} - 3H$ complexes, that are likely present in MOVPE-grown GaN. Degradation of GaN-based optical devices, operating under high current densities, has been widely reported [103, 104]. Since the V_{Ga} activation involves high beam current density induced by LEEBI, it is also plausible that the same mechanism is present in degradation of GaN-based optical devices during high current density operation.

In the future, samples grown with different methods than MOVPE will be studied. Especially, using plasma-assisted MBE, GaN can be grown without any hydrogen present (aside from possible contamination). This way it might be possible to gain more insight into the vacancy passivation mechanism. The formation of the in-grown V_{Ga} (in MOVPE) might be avoidable with optimized growth conditions, hence reducing the LEEBI sensitivity of GaN-based components. Furthermore, the effect of a high charge injected by a current source will be studied. If any PL intensity degradation can be found and linked to the vacancy activation it would confirm the similarities of the degradation of both e-beam irradiated and electrically injected GaN. Moreover, there are several factors affecting the formation of gallium vacancies, which could all be studied, such as the lattice orientation and the Fermi level. There are also measurement techniques (*e.g.*, deep-level transient spectroscopy (DLTS), Hall

effect and EBIC) that can be used to reveal details of irradiated GaN. For example, DLTS might be particularly useful in determining the energy level of the activated vacancies. Also, more detailed studies on possible contributions from other kinds of defects and vacancy complexes will be carried out.

Despite the degrading action caused by LEEBI during EBL, silver nano-patterned grating on top of a GaN/InGaN/GaN near-surface QW structure still exhibited amplification of extraction efficiency. The best results were obtained using a silver stripe pattern buried in PVA. Up to 2.8-fold increase in PL intensity was obtained compared to a non-patterned sample. Thus, this technique shows great promise to increase the efficiency of (GaN-based) light emitting devices.

Further improvement of the nano-grating technique should be straightforward with optimized layer thicknesses, grating periods and cover materials. Especially, if the LEEBI induced degradation can be reduced, higher light extraction is to be expected. This could be achieved, *e.g.*, with higher acceleration voltage in EBL, or by using substitutive lithography technique such as laser interference lithography or nano-imprint lithography. Extraction enhancement using plasmonic coupling should be achievable with optimized grating period or the plasmonic coupling can even be disregarded and the optimization done only for the waveguide mode diffraction.

Moreover, studies on novel structures possibly allowing efficient electrical pumping of the near-surface quantum well LEDs has begun. The technique is based on carrier diffusion and can allow new kinds of ways to realize electrical excitation in problematic configurations such as nanowires and plasmonic structures.

Bibliography

[1] O. V. Losev. Luminous carborundum detector and detection with crystals. *Telegrafiya i Telefoniya bez Provodov*, 44:485–494, 1927.

[2] R. Braunstein. Radiative transitions in semiconductors. *Physical Review*, 99(6):1892, 1955.

[3] N. Holonyak and S. F. Bevacqua. Coherent (visible) light emission from ga($as_{1-x}p_x$) junctions. *Applied Physics Letters*, 1(4):82, 1962.

[4] N. Zheludev. The life and times of the led - a 100-year history. *Nature Photonics*, 1:189–192, 2007.

[5] F.K. Yam and Z. Hassan. Innovative advances in led technology. *Microelectronics Journal*, 36(2):129, 2005.

[6] Komine, T. and Nakagawa, M. . Integrated system of white led visible-light communication and power-line communication. *IEEE Transactions on Consumer Electronics*, 49(1):71, 2003.

[7] H. X. Jiang. Iii-nitride blue microdisplays. *Applied Physics Letters*, 78(9):1303, 2001.

[8] R. Dingle and K. L. Shaklee and R. F. Leheny and R. B. Zetterstrom. Stimulated emission and laser action in gallium nitride. *Applied Physics Letters*, 19(1):5, 1971.

[9] Glenn Zorpette. Let there be light. *IEEE Spectrum*, pages 70–74, 2002.

[10] S. Pearton and J. Zolper and R. Shul and F. Ren. Gan: Processing, defects, and devices. *Journal of Applied Physics*, 86:78, 1999.

[11] S. Nakamura and M. Senoh and S. Nagahama and N. Iwasa and T. Yamada and T. Maatsushita and H. Kijoku and Y. Sugimoto. Ingan-based multi-quantum-well-structure laser diodes. *Japanese Journal of Applied Physics*, 35:L74, 1996.

[12] J. Wu and W. Walukiewich and K. M. Yu and J. W. AgerIII Li and E. E. Haller and H. Lu and W. J. Schaff. Superior radiation resistance of $in_{1-x}ga_xn$ alloys: Full-solar-spectrum photovoltaic material system. *Journal of Applied Physics*, 94(10):6477, 2003.

[13] Omkar Jani and Ian Ferguson and Christiana Honsberg and and Sarah Kurtz. Design and characterization of gan/ingan solar cells. *Applied Physics Letters*, 91(13):132117, 2007.

[14] Ray-Hua Horng and Shih-Ting Lin and Yu-Li Tsai and Mu-Tao Chu and Wen-Yih Liao and Ming-Hsien Wu and Ray-Ming Lin and Yuan-Chieh Lu. Improved conversion efficiency of gan/ingan thin-film solar cells. *IEEE Electron Device Letters*, 30(7):724, 2009.

[15] Shuji Nakamura and Masayuki Senoh and Naruhito Iwasa and Shin-ichi Nagahama and Takao Yamada and Takashi Mukai. Superbright green ingan single-quantum-well-structure light-emitting diodes. *Japanese Journal of Applied Physics*, 34:1332, 1995.

[16] M. D. Drory and J. W. Ager III and T. Suski and I. Grzegory and S. Porowski. Hardness and fracture toughness of bulk single crystal gallium nitride. *Applied Physics Letters*, 69(26):4044, 1996.

[17] A. F. Wright. Elastic properties of zinc-blende and wurtzite aln, gan, and inn. *Journal of Applied Physics*, 82(6):2833, 1997.

[18] Yi-Feng Wu and David Kapolnek and James P. Ibbetson and Primit Parikh and Bernd P. Keller and Umesh K. Mishra. Very-high power density algan/gan hemts. *IEEE Transactions On Electronic Devices*, 48(3):586–590, 2001.

[19] D. Walker and E. Monroy and P. Kung and J. Wu and M. Hamilton and F. J. Sanchez and J. Diaz and M. Razeghi. High-speed, low-noise metal–semiconductor–metal ultraviolet photodetectors based on gan. *Applied Physics Letters*, 74(5):762, 1999.

[20] L. F. Eastman and U. K. Mishra. The toughest transistor yet [gan transistors]. *IEEE Spectrum*, 39(5):28, 2002.

[21] P.J. Sellina and J. Vaitkus. New materials for radiation hard semiconductor dectectors. *Nuclear Instruments and Methods in Physics Research A*, 557:479, 2006.

[22] P. Bhattacharya. *Semiconductor Optoelectronic Devices*. Pearson Education Company, 2nd edition, 1997.

[23] Yi-Feng Wu and D. Kapolnek and J. P. Ibbetson and P. Parikh and B. P. Keller and U. K. Mishra. Very-high power density algan/gan hemts. *IEEE Transactions on Electron Devices*, 48(3):586, 2001.

[24] T. Palacios and A. Chakraborty and S. Rajan and C. Poblenz and S. Keller and S. P. DenBaars and J. S. Speck and U. K. Mishra. High-power algan/gan hemts for ka-band applications. *IEEE Electron Device Letters*, 26(11):781, 2005.

[25] M. Leszczynski and H. Teisseyre and T. Suski and I. Grzegory and M. Bockowski and J. Jun and S. Porowski and K. Pakula and J. M. Baranowski and C. T. Foxon and and T. S. Cheng. Lattice parameters of gallium nitride. *Applied Physics Letters*, 69(1):73, 1996.

[26] R. Dahal and B. Pantha and J. Li and J. Y. Lin and H. X. Jiang. Ingan/gan multiple quantum well solar cells with long operating wavelengths. *Applied Physics Letters*, 94(6):063505, 2009.

[27] C. J. Neufeld and N. G. Toledo and S. C. Cruz and M. Iza and S. P. DenBaars and U. K. Mishra. High quantum efficiency ingan/gan solar cells with 2.95 ev band gap. *Applied Physics Letters*, 93(14):143502, 2008.

[28] A. Cros and R. Dimitrov and H. Angerer and O. Ambacher and M. Stutzmann and S. Christiansen and M. Albrecht and H.P. Strunk. Influence of magnesium doping on the structural properties of gan layers. *Journal of Crystal Growth*, 181(3):197, 1997.

[29] A. Kasi Viswanath and Eun-joo Shin and Joo In Lee and Sungkyu Yu and Dongho Kim and Baeyong Kim and Yoonho Choi and and Chang-Hee Hong. Magnesium acceptor levels in gan studied by photoluminescence. *Journal of Applied Physics*, 83(4):2272, 1998.

[30] L. B. Rowland and K. Doverspike and D. K. Gaskill. Silicon doping of gan using disilane. *Applied Physics Letters*, 66(12):1495, 1995.

[31] A. Cremades and L. Görgens and O. Ambacher and M. Stutzmann and F. Scholz . Structural and optical properties of si-doped gan. *Physical Review B*, 61:2812, 2000.

[32] X. Guo and X. Wang and B. Chang and Y. Zhang and Pin Gao. High quantum efficiency of depth grade doping negative-electron-affinity gan photocathode. *Applied Physics Letters*, 97(6):063104, 2010.

[33] C.I. Wu and A. Kahn. Negative electron affinity and electron emission at cesiated gan and aln surfaces. *Applied Surface Science*, 162-163:250, 2000.

[34] C. Sevik and C. Bulutay. Gunn oscillations in gan channels. *Semiconductor Science and Technology*, 19:188, 2004.

[35] S. Nakamura and G. Fasol. *The Blue Laser Diode: GaN based light emitters and lasers*. Springer-Verlag Berlin Heidelberg, 1997.

[36] C. M. Lueng and H. L. W. Chan and C. Surya and C. L. Choy. Piezoelectric coefficiet of aluminum nitride and gallium nitride. *Journal of Applied Physics*, 99(9):5360, 2000.

[37] S. Muensit and I. L. Guy. The piezoelectric coefficient of gallium nitride thin films. *Journal of Applied Physics*, 72(15):1896, 1998.

[38] Stephen Gasiorowicz. *Quantum Physics*. Wiley, 3 edition, 2003.

[39] C. Weisbuch and B. Vinter. *Quantum Semiconductor Structures: Fundamentals and Applications*. Academic Press Limited, 1991.

[40] David J. Griffits. *Introduction to Quantum Mechanics*. Pearson Education International, international edition, 2005.

[41] J. Singh. *electronic and Optoelectronic Properties of Semiconductor Structures*. Cambridge University Press, 2003.

[42] P. Boguskawski and E. L. Briggs and J. Bernholc. Native defects in gallium nitride. *Physical review B*, 51(23):255–258, 1995.

[43] K. Leung and A. F. Wright and E. B. Stechel. Charge accumulation at a threading edge dislocation in gallium nitride. *Applied Physics Letters*, 74(17):2495, 1999.

[44] C. H. Qiu and C. Hoggatt and W. Melton and M. W. Leksono and J. I. Pankove. Study of defect states in gan films by photoconductivity measurement. *Applied Physics Letters*, 66(20):2712, 1995.

[45] M. G. Ganchenkova and R. M. Nieminen. Nitrogen vacancies as major point defects in gallium nitride. *Physical Review Letters*, 96:196402, 2006.

[46] Jörg Neugebauer and Chris G. Van de Walle. Gallium vacancies and the yellow luminescence in gan. *Applied Physics Letters*, 69:503, 1996.

[47] J. Oila and J. Kivioja and V. Ranki and K. Saarinen and D. C. Look and R. J. Molnar and S. S. Park and S. K. Lee and J. Y. Han. Ga vacancies as dominant intrinsic acceptors in gan grown by hydride vapor phase epitaxy. *Applied Physics Letters*, 82(20):3433, 2003.

[48] T. L. Tansley and R. J. Egan. Point-defect energies in the nitrides of aluminum, gallium, and indium. *Physical Review B*, 45(19):10942, 1992.

[49] Martin F. Schubert and Sameer Chhajed and Jong Kyu Kim and and E. Fred Schubert and Daniel D. Koleske and Mary H. Crawford and Stephen R. Lee and Arthur J. Fischer and Gerald Thaler and Michael A. Banas. Effect of dislocation density on efficiency droop in gainn/gan light-emitting diodes. *Applied Physics Letters*, 91:231114, 2007.

[50] S. Y. Karpov and Y. N. Makarov. Dislocation effect on light emission efficiency in gallium nitride. *Applied Physics Letters*, 81(25):4721, 2002.

[51] J. Elsner and R. Jones and P. K. Sitch and V. D. Porezag and M. Elstner and Th. Frauenheim and M. I. Heggie and S. Öberg and P. R. Briddon . Theory of threading edge and screw dislocations in gan. *Physical Review Letters*, 79(19):3672, 1997.

[52] Hui-Youn Shin and S.K. Kwon and Y.I. Chang and M.J. Cho and K.H. Park. Reducing dislocation density in gan films using a cone-shaped patterned sapphire substrate. *Journal of Crystal Growth*, 311(17):4167, 2009.

[53] Qiming Li and Jeffrey J. Figiel and George T. Wang. Dislocation density reduction in gan by dislocation filtering through a self-assembled monolayer of silica microspheres. *Applied Physics Letters*, 94(23):231105, 2009.

[54] X. Q. Shen and H. Matsuhata and H. Okumura. Reduction of the threading dislocation density in gan films grown on vicinal sapphire (0001) substrates. *Applied Physics Letters*, 86(2):021912, 2005.

[55] J. Chaudhuri, J. T. George, D. D. Kolske, A. E. Wickenden, R. L. Henry, Z. Rek. Reduction of dislocation density in gan films on sapphire using ain interlayers. *Journal of Materials Science*, 37(7):1449, 2002.

[56] J. Chaudhuri, J. T. George, D. D. Kolske, A. E. Wickenden, R. L. Henry, Z. Rek. Fabrication and characterization of low defect density gan using facet-controlled epitaxial lateral overgrowth (facelo). *Journal of Crystal Growth*, 221(1-4):316, 2000.

[57] Fanciulli, Marco and Molnar, Richard J. and Moustakas, Theodore D. and Graham, R. J. and Scanlon, J. . Epitaxial growth of zinc blende and wurtzitic gallium nitride thin films on (001) silicon. *Applied Physics Letters*, 59:944–946, 1991.

[58] Wentao Jua and Daniel A. Gulinoa and Ryan Higgins. Epitaxial lateral overgrowth of gallium nitride on silicon substrate. *Journal of Crystal Growth*, 263(1-4):30–34, 2004.

[59] S. Yoshida and S. Misawa and S. Gonda. Improvements on the electrical and luminescent properties of reactive molecular beam epitaxially grown gan films by using alncoated sapphire substrates. *Applied Physics Letters*, 42:427, 1983.

[60] F. Tuomisto and K. Saarinen and B. Lucznik and I. Grzegory and H. Teisseyre and T. Suski and S. Porowski and P. R. Hageman and and J. Likonen. Effect of growth polarity on vacancy defect and impurity incorporation in dislocation-free gan. *Applied Physics Letters*, 86(3):031915, 2005.

[61] M. Rummukainen and J. Oila and A. Laakso and K. Saarinen and A. J. Ptak and and T. H. Myers. Vacancy defects in o-doped gan grown by molecular-beam epitaxy: The role of growth polarity and stoichiometry. *Applied Physics Letters*, 84(24):4887, 2003.

[62] M. A. Reshchikov and H. Morkoç. Luminescence properties of defects in gan. *Journal of Applied Physics*, 97:061301, 2005.

[63] S. Hautakangas and V. Ranki and I. Makkonena and M. J. Puska and K. Saarinen and L. Liszkay and D. Seghier and H. P. Gislason and J.A. Freitas and R.L. Henry and X. Xu and D.C. Look. Gallium and nitrogen vacancies in gan: Impurity decoration effects. *Physica B*, 376-377:424, 2006.

[64] D.C Look and D.C Reynoldsa and Z.-Q Fanga and J.W Hemskya and J.R Sizeloveb and R.L Jonesb. Point defect characterization of gan and zno. *Materials Science and Engineering: B*, 66:30, 1999.

[65] K. Laaksonen and M. G. Ganchenkova and R. M. Nieminen. Vacancies in wurtzite gan and aln. *Journal of Physics: Condensed Matter*, 21:015803, 2009.

[66] D. C. Look and G. C. Farlow and P. J. Drevinsky and D. F. Bliss and and J. R. Sizelove. On the nitrogen vacancy in gan. *Applied Physics Letters*, 83(17):3525, 2003.

[67] K. Saarinen and T. Laine and S. Kuisma and J. Nissilä and P. Hautojärvi and L. Dobrzynski and J. M. Baranowski and K. Pakula and R. Stepniewski and M. Wojdak and A. Wysmolek and T. Suski and M. Leszczynski and I. Grzegory and S. Porowski. Observation of native ga vacancies in gan by positron annihilation. *Physical Review Letters*, 79(16):3030, 1997.

[68] T. Mattila and R. M. Nieminen. Point-defect complexes and broadband luminescence in gan and aln. *Physical Review B*, 55(15):9571–9576, 1997.

[69] I. Gorczyca and N. E. Christensen and A. Svane. Influence of hydrostatic pressure on cation vacancies in gan, aln, and gaas. *Physical Review B*, 66(7):075210, 2002.

[70] J. Oila and V. Ranki and J. Kivioja and K. Saarinen and P. Hautojärvi and J. Likonen and J. M. Baranowski and K. Pakula and T. Suski and M. Leszczynski and I. Grzegory. Influence of dopants and substrate material on the formation of ga vacancies in epitaxial gan layers. *Physical Review B*, 63:045205, 2001.

[71] S. Limpijumnong and C. G. Van der Walle. Diffusivity of native defects in gan. *Physical Review B*, 69(3):035207, 2004.

[72] Jörg Neugebauer and Chris G. Van de Walle. Hydrogen in gan: Novel aspects of a common impurity. *Physical Review Letters*, 75(24):4452–4455, 1995.

[73] A. F. Wright and C. H. Seager and S. M. Myers and D. D. Koleske and A. A. Allerman. Hydrogen configurations, formation energies, and migration barriers in gan. *Journal of Applied Physics*, 94(4):2311, 2003.

[74] Chris G. Van de Walle. Hydrogen as a shallow center in semiconductors and oxides. *Physica Status Solidi B*, 235(1), 89-95 2003.

[75] A. F. Wright. Interaction of hydrogen with gallium vacancies in wurtzite gan. *Journal of Applied Physics*, 90:1164, 2001.

[76] Chris G. Van de Walle. Interactions of hydrogen with native defects in gan. *Physical Review B*, 56(16):R10020–R10023, 1997.

[77] S. Nakamura and N. Iwasa and M. Senoh and Takashi Mukai. Hole compensation mechanism of p-type gan films. *Japanese Journal of Applied Physics*, 31:1258–1266, 1992.

[78] T. Mattila and R. M. Nieminen . Ab initio study of oxygen point defects in gaas, gan, and aln. *Physical Review B*, 54(23):16676, 1996.

[79] T. Ogino and M. Aoki. Mechanism of yellow luminescence in gan. *Japanese Journal of Applied Physics*, 19(12):2395, 1980.

[80] H. Amano and M. Kito and K. Hiramatsu and I. Akasaki. P-type conduction in mg-doped gan treated with low-energy electron beam irradiation (leebi). *Japanese Journal of Applied Physics*, 28:L2112–2114, 1989.

[81] S. Hautakangas and I. Makkonen and V. Ranki and M. J. Puska and K. Saarinen. Direct evidence of impurity decoration of ga vacancies in gan from positron annihilation spectroscopy. *Physical Review B*, 73:193391, 2006.

[82] H. D. Young and R. A. Freedman. *University Physics*. Addison Wesley Longman; 10th ed., 2000.

[83] Z.-J. Ding and R. Shimizy. A monte carlo modeling of electron interaction with solids including cascade secondary electron production. *Scanning*, 18:92–113, 1996.

[84] H. Schwenke and J. Knoth. A highly sensitive energy-dispersive x-ray spectrometer with multiple total reflection of the exciting beam. *Nuclear Instruments and Methods in Physics Research*, 193(1-2):239–243, 1982.

[85] A. R. Couture and D. Drouin. Casino v2.48. 2000. Complex single scattering Monte Carlo program.

[86] H. Demers, N. Poirier-Demers, A. R. Couture, D. Joly, M. Guilmain, N. de Jonge, D. Drouin. Three-dimensional electron microscopy simulation with the casino monte carlo software. *Scanning*, 33(3):135–146, 2011.

[87] T. Everhart and P. H. Hoff. *Journal of Applied Physics*, 42:5837, 1971.

[88] O. Kurniawan and V. K. S. Ong. Investigation of range-energy relationships for low-energy electron beams in silicon and gallium nitride. *Scanning*, 29:280, 2007.

[89] W. A. McKinley and H. Feshbach. The coulomb scattering of relativistic electrons by nuclei. *Physics Review*, 74(12):1759–1763, 1948.

[90] F. Tuomisto and V. Ranki and D. C. Look abd G. C. Farlow. Introduction and recovery of ga and n sublattice defects in electron-irradiated gan. *Physical Review B*, 76(16):165207, 2007.

[91] D. B. Williams and C. B. Carter. *The Transmission Electron Microscope*. Springer US, 1996.

[92] M. Ali and O. Svensk and Z. Zhen and S. Suihkonen and P.T. Törmä and H. Lipsanen and M. Sopanen and K. Hjort and J. Jensen. Reduced photoluminescence from ingan/gan multiple quantum well structures following 40 mev iodine ion irradiation. *Physica B: Condensed Matter*, 404(23-24):4925–4928, 2009.

[93] K. A. Mkhoyan and J. Silcox. Electron-beam-induced damage in wurtzite inn. *Applied Physics Letters*, 82(6):859, 2003.

[94] J. Singh. *Semiconductor Optoelectronics*. McGraw-Hill International Editions, 1995.

[95] H. Amano and N. Sawaki and I. Akasaki and Y. toyoda. Metalorganic vapor phase epitaxial growth of a high quality gan film using an aln buffer layer. *Applied Physics Letters*, 48(5):353, 1986.

[96] R. W. Siegel. Positron annihilation spectrosopy. *Annual Review of Materials Science*, 10:8654, 1980.

[97] B. Y. Tong. Negative work function of thermal positrons in metals. *Physical Review B*, 5(4):1436–1439, 1972.

[98] Peter J. Schultz and K. G. Lynn. Interaction of positron beams with surfaces, thin films, and interfaces. *Review of Modern Physics*, 60(3):701–779, 1988.

[99] F. Tuomisto and T. Paskova and R. Kröger and S. Figge and D. Hommel and B. Monemar and R. Kersting. Defect distribution in a-plane gan on al_2o_3. *Applied Physics Letters*, 90:121915, 2007.

[100] M. T. Postek. An approach to the reduction of hydrocarbon contamination in the scanning electron microscope. *Scanning*, 18:269, 1996.

[101] T. Li and E. Hahn and D. Gerthsen and A. Rosenauer and A. Strittmatter and L. Reißmann and and D. Bimberg. Indium redistribution in an ingan quantum well induced by electron-beam irradiation in a transmission electron microscope. *Applied Physics Letters*, 86(24):241911, 2005.

[102] T. M. Smeeton and C. J. Humphreys and J. S. Barnard and M. J. Kappers. The impact of electron beam damage on the detection of indium-rich localisation centres in ingan quantum wells using transmission electron microscopy. *Journal of Materials Science*, 41(9):2729, 2006.

[103] M. Meneghini and G. Meneghesso and N. Trivellin and E. Zanoni and K. Orita and M. Yuri and D. Ueda. Extensive analysis of the degradation of blu-ray laser diodes. *IEEE Electron Device Letters*, 29(6):578, 2008.

[104] Michael Kneissl and David P. Bour and Linda Romano and Chris. G. Van de Walle and John E. Northrup and William S. Wong and David W. Treat and Mark Teepe and Tanya Schmidt and Noble M. Johnson. Performance and degradation of continuous-wave ingan multiple-quantum-well laser diodes on epitaxially laterally overgrown gan substrates. *Applied Physics Letters*, 77(13):1931, 2000.

[105] L. Marona and P. Wisniewski and P. Prystawko and I. Grzegory and T. Suski and S. Porowski and P. Perlin and R. Czernecki and and M. Leszczyński. Degradation mechanisms in ingan laser diodes grown on bulk gan crystals. *Applied Physics Letters*, 88(20):201111, 2006.

[106] F. J. Xu and B. Shen and L. Lu and Z. L. Miao and J. Song and Z. J. Yang and G. Y. Zhang and X. P. Hao and B. Y. Wang and X. Q. Shen and H. Okumura. Different origins of the yellow luminescence in as-grown high-resistance gan and unintentional-doped gan films. *Journal of Applied Physics*, 107(2):023528, 2010.

[107] Y. Kawakami and Y. Narukawa and K. Omae and Sg. Fujita and S. Nakamura. Dimensionality of excitons in ingan-based light emitting devices. *Physica Status Solidi A*, 178(1):331–336, 2000.

[108] J. J. Wierer and M. R. Krames and J. E. Epler and N. F. Gardner and M. G. Craford and J. R. Wendt and J. A. Simmons and M. M. Sigalas. Ingan/gan quantum-well heterostructure light-emitting diodes employing photonic crystal structures. *Applied Physics Letters*, 84(19):3885, 2004.

[109] C. Hums and T. Finger and T. Hempel and J. Christen and A. Dadgar and A. Hoffmann and A. Krost. Fabry-perot effects in ingan/gan heterostructures on si-substrate. *Journal of Applied Physics*, 101(3):033133, 2007.

[110] M. A. Mastro and J. D. Caldwell and R. T. Holm and R. L. Henry and C. R. Eddy Jr. Design of gallium nitride resonant cavity light-emitting diodes on si substrates. *Advanced Materials*, 20(1):115–118, 2008.

[111] M. Ali and O. Svensk and L. Riuttanen and M. Kruse and S. Suihkonen and A .E. Romanov and P. T. Törmä and M. Sopanen and H. Lipsanen and M.A. Odnoblyudov and V. E. Bougrov. Enhancement of near-uv gan led light extraction efficiency by gan/sapphire template patterning. *Semiconductor Science and Technology*, 27:082002, 2012.

[112] A. David and T. Fujii and R. Sharma and K. McGroddy and S. Nakamura and S. P. DenBaars and E. L. Hu and C. Weisbuch and H. Benisty. Photonic-crystal gan light-emitting diodes with tailored guided modes distribution. *Applied Physics Letters*, 88(6):061124, 2006.

[113] J. J. Wierer Jr. and A. David and M. M. Megens. Iii-nitride photonic-crystal light-emitting diodes with high extraction efficiency. *Nature Photonics*, 3:163–169, 2009.

[114] Kwan Hyun Cho and Sung Il Ahn and Seong Min Lee and Chung Sock Choi and Kyung Cheol Choi. Surface plasmonic controllable enhanced emission from the intrachain and interchain excitons of a conjugated polymer. *Applied Physics Letters*, 97(19):193306, 2010.

Aalto-DD 190/2013

ISBN 978-952-60-5444-5
ISBN 978-952-60-5445-2 (pdf)
ISSN-L 1799-4934
ISSN 1799-4934
ISSN 1799-4942 (pdf)

Aalto University
School of Electrical Engineering
Department of Micro- and Nanosciences
www.aalto.fi

BUSINESS +
ECONOMY

ART +
DESIGN +
ARCHITECTURE

SCIENCE +
TECHNOLOGY

CROSSOVER

DOCTORAL
DISSERTATIONS